Engineering nanoparticle communication in living systems by stigmergy: An application to enhance antitumor therapy in triple-negative breast cancer

Alejandra Estepa-Fernández [a,b,c], Alba García-Fernández [a,b,c,*], Araceli Lérida-Viso [a,b,c,d], Angela Morellá-Aucejo [a,b,c], Juan José Esteve-Moreno [a,b,c], Juan F. Blandez [a,b,c,d], María Alfonso [a], Vicente Candela-Noguera [a,b], Gema Vivo-Llorca [a,b], Félix Sancenon-Galarza [a,b,c,d], Mar Orzáez [b,e], Ramón Martínez-Máñez [a,b,c,d,*]

[a] *Instituto Interuniversitario de Investigación de Reconocimiento Molecular y Desarrollo Tecnológico (IDM) Universitat Politècnica de València, Universitat de València, Camino de Vera, s/n, 46022 Valencia, Spain*
[b] *Unidad Mixta UPV-CIPF de Investigación en Mecanismos de Enfermedades y Nanomedicina, Universitat Politècnica de València, Centro de Investigación Príncipe Felipe, C/ Eduardo Primo Yúfera 3, 46012 Valencia, Spain*
[c] *CIBER de Bioingeniería, Biomateriales y Nanomedicina (CIBER-BBN), Spain*
[d] *Unidad Mixta de Investigación en Nanomedicina y Sensores. Universitat Politècnica de València, IIS La Fe, Av. Fernando Abril Martorell, 106 Torre A 7ª planta, 46026 Valencia, Spain*
[e] *Centro de Investigación Príncipe Felipe, C/ Eduardo Primo Yúfera 3, 46012 Valencia, Spain*

[*] Corresponding authors at: Instituto Interuniversitario de Investigación de Reconocimiento Molecular y Desarrollo Tecnológico (IDM) Universitat Politècnica de València, Universitat de València, Camino de Vera, s/n, 46022 Valencia, Spain.
E-mail addresses: algarfe4@etsia.upv.es (A. García-Fernández), rmaez@qim.upv.es (R. Martínez-Máñez).

***Keywords**:* Nanoparticle communication Mesoporous silica nanoparticles Senescence, Navitoclax, Palbociclib, TNBC

Abstract: The engineering of nanoparticle communication has gained growing attention in the last years, however, efforts to communicate nanoparticles with living systems is still a barely studied emerging topic. Here, we explore a nanoparticle cooperation strategy that involves nanoparticle-cell-nanoparticle communication in vivo through stigmergy (a strategy in which nanodevices communicate by modifying the environment). First, mesoporous silica nanoparticles loaded with the senescence inductor palbociclib and coated with a heterobifunctional poly(ethylene glycol) that binds covalently to a MUC1-binding aptamer (NP(palbo)PEG- MUC1), is designed to specifically deliver the pro-senescent drug palbociclib in MDA-MB-231 breast cancer cells. Once the first nanoparticle modifies the environment due to the induction of senescence, a second community of nanoparticles, loaded with the senolytic navitoclax and coated with a hexa-oligo-saccharide (NP(nav)-Gal), releases its cargo to eliminate tumor senescent cells selectively. The targeted therapy through stigmergy communication is tested in vitro, and in vivo, where delays tumor growth and reduces metastases in a mouse model of human triple-negative breast cancer while minimizing undesired drugs side effects.

Introduction

Since the introduction of the concept of nanotechnology several years ago, a number of nanoparticles for different applications in areas such as medicine, biotechnology, environmental science, sen- sing, etc., have been reported and today, it is possible to design complex nanoparticles for selected purposes [1]. However, no matter what the context is, reported nanodevices are usually studied as single non-interactive systems, yet communication involving nano- particles is a scarcely studied topic. However, establishing the foundations for communication between nanoparticles, and nano- particles with cells, may expand their potential use in advanced applications allowing them to share information and cooperate [2]. The concept of communication is essential in living systems and has been crucial for the development of information and communication technologies at the macroscale. In contrast, communication between nanoparticles or nanoparticles with cells is not an easy task and traditional communication technologies are not trivial to apply. A potential approach for establishing communication is to mimic how nature communicates via the use of chemical messengers [3,4]. It is in fact, the use of molecular messengers the main mechanism of communication in nature, and it is ubiquitously used by biological systems. However, very few examples have been reported where micro/nanosystems communicate via the interchange of chemical messengers using different enabling technologies, which can be classified by the micro/nanoparticles (giant liposomes, proteinosomes, coacervates, mesoporous silica, etc.) and by the information processing tools used(cell-free transcription-translation machinery (TXTL), DNA displacement reactions, enzymes and responsive molecular ensembles) [4–12].

In addition, in contrast to the interchange of chemical messengers, many swarm systems in nature communicate by modifying the environment, a concept that is termed stigmergy [13]. In this communication protocol, the trace left by an action in a medium stimulates subsequent actions. The concept of stigmergy has been used to analyze self-organizing activities in a wide range of domains, including robotics, web communities, human society and social in- sects.[14] Stigmergy communication examples in nature involve ants that deposit and sense chemical signals to find food or in termites that can build complex structures by modifying their physical environment [15]. Despite its great potential, the stigmergy paradigm has still been poorly studied in nanotechnology, however, it em- braces a completely different mode of communication that can result in several applications and advances in the way we use and design nanoparticles. In this communication protocol one can picture different communities of nanoparticles one of which performs an action and the trace of this action on the

medium stimulates the performance of the second community of particles. However, despite its potential its full power remains underappreciated and examples using nanoparticles and living systems remains almost un- explored [16,17].

Based on the high potential of the stigmergy concept and considering our interest in the design of communication protocols in- volving nanoparticles,[2,6–8,18,19] we report herein a stigmergic nanoparticle-cell/tumor-nanoparticle communication applied to enhance tumor therapy in triple-negative breast cancer in vivo (**Fig. 1**) taking advantage of the transformation of tumor cells to senescent cells. Briefly, senescence is a cellular state of cell cycle arrest that has traditionally been thought to function as a physio- logical barrier against tumorigenesis [20–22]. However, the accumulation of senescent cells in tumors has been reported to have deleterious effects [23–27]. Therefore, we envisioned the use of a first population of nanoparticles able to transform tumor cells in senescent cells (transformation of the environment) combined by a second community of nanoparticles able to eliminate senescent cells, with the aim to reduce tumor size by stigmergy. Among senescence-inducing compounds, we used palbociclib, a cyclin-de- pendent kinase (CDKs) inhibitor already in clinical use [28–31]. In relation to senolytic drugs, we used navitoclax, which has shown effectiveness in vivo in eliminating senescent cells.[32–35] As a consequence of the cooperation by stigmergy of both nanoparticles, tumor growth reduction, drop of metastases and diminution of drug side effects is observed in a triple-negative breast cancer mice model.

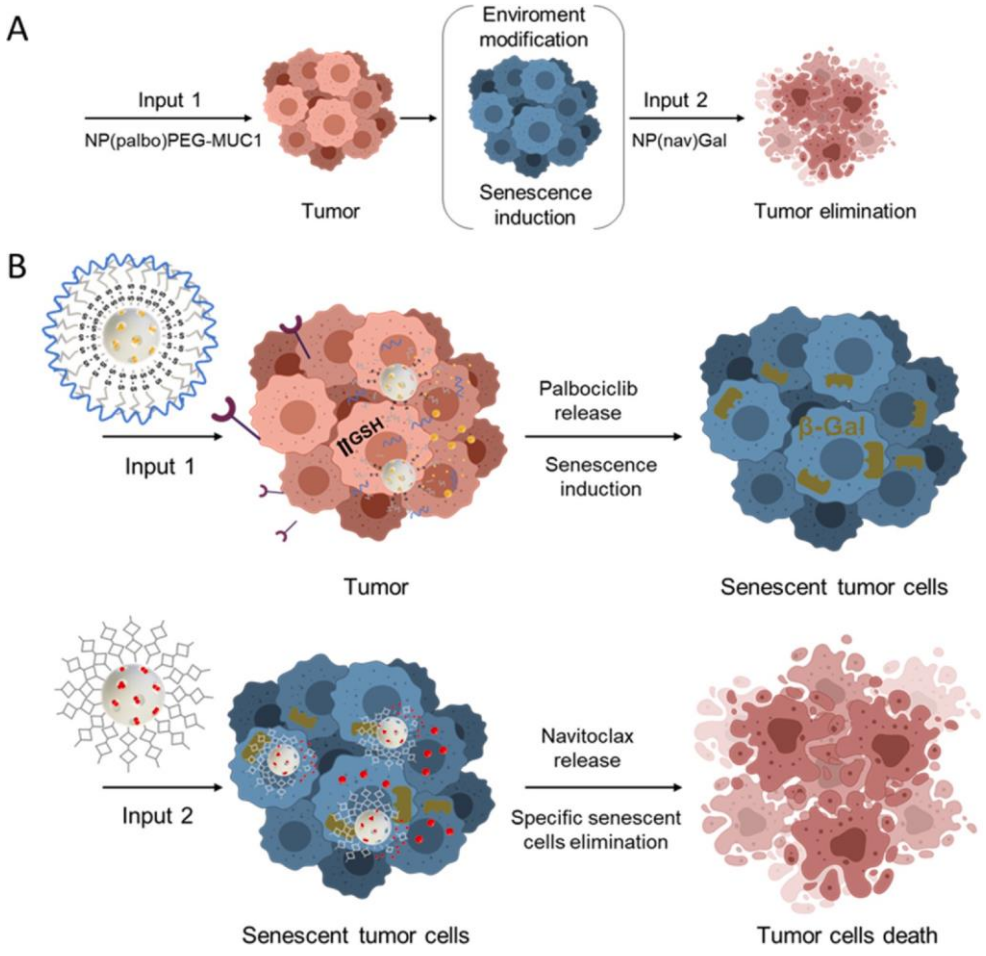

Fig. 1. Nanoparticle communication by stigmergy for enhanced tumor reduction using targeted induction of senescence and senolysis. (A) Schematic representation of stigmergy communication concept. A first community of nanoparticles induces a modification in the environment in such a way that enhanced the action of a subsequent community of nanoparticles. (B) **NP(palbo)PEG-MUC1** (first community of nanoparticles) releases its cargo in cancer cells due to both (1) the presence of a MUC1-binding aptamer and (2) a high intracellular concentration of glutathione (GSH) that reduces the disulfide bonds of the capping PEG. The release of palbociclib by the first community of nanoparticles modifies the environment by senescence induction in tumor cells. This allows a second community of nanoparticles (NP(nav)-Gal) release their content in senescent cells due to their high lysosomal β-galactosidase activity. β-Galactosidase induces the hydrolysis of the capping ensemble (galactan) with subsequent delivery of a senolytic cargo (navitoclax) that eliminates senescent by apoptosis reducing tumor size.

Materials and methods

Cell culture and senescence induction

Human breast triple-negative adenocarcinoma MDA-MB-231 cells (ATCC) were maintained in DMEM (Sigma) supplemented with 10% fetal bovine serum (FBS; Sigma) and incubated at 37 °C in 5% CO_2. For senescence induction, cells were treated with 2.5 μM free palbociclib (Pfizer) or with 80 μg/mL **NP(palbo)PEG-MUC1** (equivalent molar dose of palbociclib than the free drug). Cells were senescent after 7 days of treatment.

β-galactosidase activity assay

β-galactosidase activity was measured by staining using the Senescence β-galactosidase Staining Kit (Cell Signaling, #9860 S). Briefly, cells were fixed with 1x Fixative Solution at room temperature for 15 min. After fixation, cells were washed with PBS and incubated overnight at 37 ºC without CO_2 with 1x Staining Solution containing X-gal in *N*,*N*-dimethylformamide. Senescence-associated β-galactosidase enzymatic activity was determined at pH 6. Pictures were taken with a bright-field microscope.

Western blot

Cells were lysed in a buffer containing 25 mM Tris-HCl pH 7.4, 1 mM EDTA, 1% SDS, plus protease and phosphatase inhibitors to obtain whole-cell extracts. Protein concentration was determined by the BCA protein assay. Electrophoresis was performed in SDS-PAGE gels. Proteins were transferred to nitrocellulose membranes, blocked with 5% nonfat milk, washed with 0.1% Tween/PBS and incubated overnight with a specific primary antibody: pRb (#9308, Cell Signaling), p21 (#sc-6246, Santa Cruz), and GADPH (#14C10, Cell Signaling). Membranes were washed and incubated with the ap-propriate secondary antibody: anti-Rabbit IgG peroxidase antibody (#A6154, Sigma) or peroxidase conjugate-goat anti-Mouse IgG an- tibody (#A4416, Sigma).

Synthesis of nanoparticles

1 g of *N*-cetyltrimethylammonium bromide (CTAB, Sigma, #H6269) was dissolved in 480 mL of deionized water before adding 3.5 mL of NaOH 2 M (Sigma, #1310732) to the solution. When the mixture was heated at 80 °C, 5 mL of the polymeric precursor tetraethylorthosilicate (TEOS, Sigma, #131903) were added dropwise and the reaction was stirred and heated for 2 h. Centrifugation (10,000 rpm, 20 min) was performed on isolated **MSNs** (white solid) that was washed with deionized water until neutral pH was reached. Finally, the solid was dried at 60 ºC and then calcined at 550 °C (Mufla Furnace) for 5 h using an oxidant atmosphere to remove the surfactant template that might affect cell viability.

Synthesis of NP(palbo)PEG-MUC1, NP(saf)PEG-MUC1 and NP(ICG) PEG-MUC1

Gated **MSNs** loaded with either palbociclib (palbo), safranine O (saf) or indocyanine green (ICG) and coated with thiol and *N*-hydroxysuccinimide heterfunctionalized polyethylene glycol (SH-PEG- NHS, average molecular weight 800 Da, Gentaur) derivative were synthesized. In order to load the pores of calcined **MSNs** with palbociclib drug, palbociclib (Pfizer) water soluble at low pH (solubility 24 mg/mL at pH 4.5) was used. 100 mg of **MSNs** were suspended in 3 mL of deionized water at pH 4.5 containing 40 mg of palbociclib-HCl. To load MSNs with safranine O, 100 mg of calcined **MSNs** were suspended in 3 mL of acetonitrile containing 28 mg of safranine O (Sigma). To load ICG, 200 mg of calcined **MSNs** were added to a stirred solution of 10 mg indocyanine green (ICG) in 50 mL of water. All the solids were stirred overnight, filtered off and dried under vacuum to obtain the loaded nanoparticles. Afterward, the loaded solids and 100 mg of empty calcined **MSNs** were suspended in acetonitrile (3 mL) and (3-mercaptopropyl) tri-methoxysilane (MPTMS) (185,6 μL, 10 mmoles/g solid), were added to the mixture and stirred for 5.5 h at room temperature. Then, 2,2'-dipyridyldisulfide (220 mg, 10 mmoles/g solid) was added and stirred overnight at room temperature. The solids were isolated by filtration, washed twice with acetonitrile and dried under vacuum. Finally, these prepared solids (100 mg) and the heterobifunctional SH-PEG-NHS (200 mg, 3 mmoles/g solid) were suspended in acet- onitrile (10 mL) and stirred overnight. The final products (**NP(palbo) PEG**, **NP(saf)PEG**, **NP(ICG)PEG** and **NP-PEG**) were filtered, washed with plenty of water and dried under vacuum.

The 5' amine-modified MUC1-binding aptamer (MUC1) (5′ NH_2- GCA GTT GAT CCT TTG GAT ACC CTG G-3'; ThermoFisher) was covalently bonded onto the external surface of **NP(palbo)PEG, NP (saf)PEG and NP(ICG)PEG**. In this respect, the solids (20 mg) were suspended in PBS and mixed with MUC1 (0,6 μmoles). The mixture was stirred for 3 h and, then nanoparticles were centrifuged and washed with PBS to get the final solids: **NP(palbo)PEG-MUC1**, **NP (saf)PEG-MUC1** and **NP(ICG)PEG-MUC1**. **NP(saf)PEG** were also coated with a 5' amine-modified non-targeting aptamer (Random) (5' NH_2-AAG CAC TTT CAG TGG GGA GGA GGG TTG ATA GGT TAA GAG-3'; ThermoFisher), that was employed as a negative control in the targeting study, obtaining the nanoparticles referred as **NP(saf) PEG-Random**. All the final nanoparticles were stored at − 20 °C.

Synthesis of NP(nav)-Gal

Synthesis of gated MSNs loaded with navitoclax (nav) or nile blue (NB) and coated with hexa-galactooligosaccharides (Active BioChem, #A1001) was performed as described previously by our group (**NP (nav)-Gal**). [26,36–38]. Besides, the synthesis of **NP(NB)-Gal** was also previously described. [39] Briefly, for navitoclax loading 200 mg of calcined **MSNs** and 156 mg navitoclax were suspended in 6 mL of anhydrous dichloromethane for 24 h. For nile blue loading 250 mg of calcined **MSNs** and 7 mg nile blue were suspended in 31 mL of an- hydrous dichloromethane for 20 h. After the loading, 0.28 mL of (3- aminopropyl) triethoxysilane were added onto the solution and stirring was kept for 5.5 h. The solid was isolated by filtration under vacuum. To obtain the final gated nanoparticles, a solution of 383 mg of galactan (Carbosynth, #OG71532, consisting of six repeating ga- lactose monosaccharides linked through β-1,4 glycosidic bonds) in 25 mL of water was added to the obtained solids functionalized, stirred at room temperature for 21 h. The final product (**NP(nav)- Gal**) was centrifuged, washed with plenty of water and ethanol in order to remove the excess of reagents and dried under vacuum. Allthe final nanoparticles were stored at room temperature in a desiccator.

Nanoparticles characterization

Powder X-ray diffraction (PXRD), N_2 adsorption-desorption isotherms, thermogravimetric analysis (TGA), transmission electron microscopy (TEM), ζ potential and dynamic light scattering (DLS) were employed for nanoparticle characterization. PXRD measure- ments were performed on a Seifert 3000TT diffractometer using Cu- Kα radiation. N_2 adsorption-desorption isotherms were recorded on a Micromeritics TriStar II Plus automated analyzer. The samples were degassed at 120 °C under vacuum overnight. The specific surface areas were calculated from the adsorption data in the low pressures range using the Brunauer–Emmett–Teller model. The thermogravimetric analyses were performed in TGA/SDTA 851e Mettler Toledo equipment in an oxidant atmosphere (air, 80 mL/min) with a heating program that consisted of a heating ramp of 10 ºC/min from 393 K to 1273 K and an isothermal heating step at this temperature for 30 min ζ potential and dynamic light scattering (DLS) measurements were carried out in a Malvern Zetasizer Nano ZS instrument. TEM images were acquired with a Philips CM10 microscope working at 100 kV. TEM-EDX analysis was performed using a JEOL-JEM-2100 LaB6 electron microscope at 200 kV accelerating voltage and equipped with an Oxford Instruments INCA x-sight (Si(Li)detector) and a Zeiss SESAM microscope(200 kV) equipped with a dispersive energy X-ray (EDX) spectroscopy system from ThermoFisher. UV–visible spectroscopy was carried out with a Lambda 35 UV/vis spectrometer (Perkin-Elmer Instruments), and cargo delivery assays were per- formed in fluorescence spectroscopy (JASCO spectrofluorometer FP- 8300). All the measurements were taken in triplicate.

Cargo release studies of NP(palbo)PEG, NP(saf)PEG and NP(ICG)PEG

1 mg of either **NP(palbo)PEG**, **NP(saf)PEG** or **NP(ICG)PEG** nanoparticles were suspended in 2 mL of water, stirred and the volume was separated in two suspensions of 1 mL. Then, 10 mM of glutathione-L-reduced (GSH) was added to one of the suspensions; the other suspension, without GSH, acts as control. After a certain time, aliquots of 150 μL of each whole suspension (including nanoparticles) were taken and centrifuged to remove the nanoparticles and maintain the supernatant for the measurement. After removing each aliquot, the whole suspension remains with the same con- centration of nanoparticles. For **NP(palbo)PEG**, cargo released was measured by UV–visible spectroscopy (absorption band of palbociclib at 352 nm). For **NP(saf)PEG** and **NP(ICG)PEG** cargo released was measured by fluorescence (λ_{exc} (saf) = 495 nm, λ_{em} (saf) = 587 nm; λ_{exc} (ICG) = 750 nm, λ_{em} (ICG) = 830 nm).

Cargo release study of NP(nav)-Gal and NP(NB)-Gal

4 mg of NP(nav)-Gal nanoparticles were suspended in 10 mL of water at pH 4.5, stirred and the volume was separated into two suspensions of 5 mL. Then, 5 mg of β-galactosidase from *Aspergillus oryzae* was added to one of the suspensions. After a certain time, aliquots of 200 μL of each whole suspension were taken, and 300 μL of ethyl acetate (to dissolve navitoclax) was added to each one. The mixture was stirred for 1 min and then centrifuged to remove the nanoparticles and maintain the supernatant for the measurement. Cargo release in the organic phases was measured by UV–visible spectroscopy (absorption band of navitoclax at 275 nm in ethyl acetate). The same procedure was performed without adding the enzyme to one of the suspensions as control.

For **NP(NB)-Gal** cargo release studies, 2 mg of **NP(NB)-Gal** was suspended in 5 mL of water-DMSO 99:1 v/v mixture at pH 4.5, in the presence or absence of 5 mg of enzyme β-galactosidase from *Aspergillus oryzae*. The suspension was stirred using a magnetic bar. Sample aliquots of 300 μL mL of the whole suspension (including nanoparticles) were taken at scheduled times and were centrifuged to remove the nanoparticles and maintain the supernatant for the measurement. Cargo release was monitored in the absorption band of NB (608 nm).

Confocal microscopy targeted cellular uptake studies

MDA-MB-231 cells were seeded on coverslips in 6-multiwell plates at a concentration of $4 \cdot 10^5$ cells/well. Two days later, cells were treated with 50 µg/mL suspension of either **NP(saf)PEG-MUC1** or **NP(saf)PEG-Random**. After 30 min, cells were washed with medium in order to eliminate non-internalized nanoparticles and were incubated for a total time of 2 h. For confocal microscopy, coverslips were mounted, Hoechst and wheat germ agglutinin (WGA) Alexa Fluor 488 were added before cells visualization for nuclei and membrane staining, respectively. Fluorescence intensity was monitored through a Leica TCS SP8 confocal microscope and quantified using Image J software.

Flow cytometry targeted cellular uptake studies

MDA-MB-231 cells were seeded in 6-multiwell plates at a con- centration of $4 \cdot 10^5$ cells/well. After 24 h, cells were treated with a suspension of 50 µg/mL of either **NP(saf)PEG-MUC1** or **NP(saf)PEG- Random**. After 30 min, cells were washed with medium in order to eliminate non-internalized nanoparticles and were incubated for different time points at 2, 4 or 6 h. Cells were collected using 0.5% Trypsin-EDTA (GIBCO) and resuspended in PBS. Flow cytometry was assessed on a CytoFlex S instrument (Beckman Coulter) followed by data analysis using CytoExpert software.

Cytotoxicity assay

Proliferating and senescent (5 µM palbociclib 7 days) MDA-MB- 231 cells were plated in flat-bottom-clear 96-well (Greiner Bio-One, #655087) at a density of 10^4 cells per well. After 24 h, free navitoclax or **NP(nav)-Gal** nanoparticles were added individually to the cells. Free navitoclax was added at a 2.5 µM final concentration. **NP(nav)- Gal** were added at a maximum of 2 mg/mL filtered (0.45 µm) which corresponds to 2.66 µM final concentration. For simultaneous co- treatment of MDA-MB-231 cells with free palbociclib plus free na- vitoclax, after 24 h of the seeding, cells were treated with 5 µM palbociclib and growing concentrations of navitoclax (0–20 µM).

In all cases, after 72 h, viability was measured using CellTiter- Glo® luminescent cell viability assay (Promega, #G7571) kit following the manufacturer's instructions in a PerkinElmer life sciences wallac Victor2TM spectrophotometer. The number of viable cells was normalized to the internal control of untreated cells (DMSO only) of each plate.

TMRE staining

For addressing mitochondrial polarization status, proliferating and senescent MDA-MB-231 cells were treated with either with DMSO, navitoclax (1 µM) or **NP(nav)-Gal** (equivalent dose to 1 µM). After 48 h of incubation, cells were incubated for 30 min at 37 °C/5% CO_2 with 50 nM TMRE dye (Invitrogen, T669). Then, samples were analyzed in a CytoFLEX S flow cytometer.

Animal experiments

All mice were treated in strict accordance with the local ethical committee (Ethical Committee for Research and Animal Welfare Generalitat Valenciana, Conselleria dÀgricultura, Medi ambient, Canvi climàtic i Desenvolupament Rural (2020/VSC/PEA/0177). In order to evaluate senolytic activity of stigmergy combination on xenografted MDA-MB-231 cells, females of 6–7 weeks old BALB/C nude mice were subcutaneously injected with 2×10^6 MDA-MB-231 cells. Tumors were measured with calipers every 2 days, and the tumor volume (mm^3) was calculated with the formula length × $width^2/2$. When tumor volume reached an average of 60 mm^3, daily therapy was initiated with either vehicle, 5 mg/kg free palbo- ciclib (via oral gavage; dissolved in 50 mM sodium lactate pH 4.5), 87.5 mg/kg **NP(palbo)PEG-MUC1** (via i.p. injection; equivalent dose of palbociclib of 5 mg/kg) or the combination of free palbociclib plus free navitoclax or **NP(palbo)PEG-MUC1** plus **NP(nav)-Gal**. Navitoclax treatments (either as a free drug or encapsulated in the nanoparticles) were initiated the day after the initiation of palbociclib treatment. Doses: 2.5 mg/kg free navitoclax (via oral gavage; dissolved in 15% DMSO/85% PEG-400) or 40 mg/kg **NP(nav)-Gal** (via i.v. and i.p. injection in alternate days; equivalent navitoclax dose of 2.5 mg/kg). Mice were culled by CO_2 after treatment, and organs were collected for subsequent histological analyses.

IVIS imaging

For *in vivo* and *ex vivo a*nimals or organs fluorescence imaging after nanoparticles treatments, an IVIS Spectrum Imaging System (Caliper LifeSciences) was used. For in vivo visualization, animals were anesthetized with 4–4.5% isoflurane in the induction period and maintained 2–2.5% during the scanning time. For *ex vivo* tumors imaging, animals were euthanized 24 h after nanoparticles injection and tumors were harvested and immediately analyzed. For **NP(ICG) PEG-MUC1** IVIS imaging, Balb/c nude female mice were injected with TNBC MDA-MB-231 cells on mammary pads. When tumors volume reached ca. 220 mm^3 (day 24 post xenograft transplanta- tion), **NP(ICG)PEG-MUC1** nanoparticles were administered (i.p.), and IVIS imaging was performed.

For **NP(ICG)-Gal** imaging, Balb/c nude female mice were injected with TNBC MDA-MB-231 cells on mammary pads. When tumors volume reached 60 mm^3 (day 10 post xenograft transplantation), palbociclib treatment started (encapsulated in **NP(palbo)PEG-MUC1** nanoparticles (i.p.) and was maintained daily for 15 days. On day 25 (post xenograft transplantation), **NP(NB)-Gal** nanoparticles were administered (i.p.), and IVIS imaging was performed. Signal from **NP**

(ICG)PEG-MUC1 nanoparticles loaded with indocyanine green were detected using excitation and emission wavelengths of 745 nm and 840 nm, respectively. Signal from **NP(NB)-Gal** nanoparticles loaded with nile blue was detected using excitation and emission wave- lengths of 640 nm and 680 nm, respectively. Fluorescence quantification was performed by Living Image® 4.3.1 software and was measured in photons per second per square centimeter per steradian ($p/s/cm^2/sr$). Fluorophore release was quantified by manually drawing regions of interest (ROIs) over the detected fluorescence signals in organs or tumors.

Histology

Tumors were removed, washed with 1 × PBS and fixed with 4% PFA overnight at 4 °C. The fixative was aspirated, the tumor was washed in 1 × PBS and cut in half. Half-tumors were incubated with 30% sucrose overnight at 4 °C. Fixed tissues were embedded in cryomolds with OCT and frozen completely at − 20 °C. 10 µm thick tumor sections were then incubated in blocking solution (5% horse serum, 0.3% Triton X-100 in 1 × PBS) for 1 h and immunostained following incubation with 1:100 p53 primary antibody (ab26, Abcam) overnight at 4 °C. Subsequently, tissue was incubated with secondary antibody (1:200 dilution) against mouse conjugated to Alexa Fluor 488 (Invitrogen) at room temperature for 2 h. For TUNEL staining, In Situ Cell Death Detection Kit (Merck) was used per the manufacturer's instructions. Sections were mounted on microscope slides using the Mowiol/DAPI (Sigma) and covered with a glass coverslip. Images were obtained using a confocal microscopy Leica TCS SP8 HyVolution 2 microscope. Positive signal for TUNEL was quantified with ImageJ software.

The other half-tumors were included in paraffin for im- munohistological Ki67 staining. 5 mm paraffin sections were de-paraffinized and re-hydrated. Antigen retrieval was carried out using 10 mM Sodium Citrate and 0.05% Tween 20 buffer at pH 6.0 for 30 min. Tumor sections were incubated in blocking solution (5% horse serum, 0.3% Triton X-100 in 1 × PBS) for 1 h and incubated with Ki67 (Abcam) antibody at 4 °C overnight. Ki67 immunostaining was developed using 3,3-diaminobenzidine tetrahydrochloride (DAB) and nuclei counterstained with hematoxylin. Sections were scanned in Leica Aperio Versa 200 equipment at 10x magnification.

Metastasis quantification

Lungs were collected and fixed overnight in 4% PFA. Paraffin- embedded tissue sections (5 µm) were stained with hematoxylin- eosin and scanned in a Leica Aperio Versa 200 equipment at 10x magnification. Metastatic 4T1 cell clusters were microscopically counted from at least five animals per group in different lung sec- tions.

Silica biodistribution

Selected organs (lungs, liver, spleen, kidneys and tumor) were extracted and conserved for silicon (Si) detection. Organs were first weighted and then individually introduced in polytetrafluoroethylene (PTFE) bottles. 1 mL of tetramethylammonium hydroxide solution (TMAH, #331635, Sigma) was added to each recipient, bottles were firmly closed, and digestion was carried out for 2 h at 80 ºC using a digestion unit Bloc digest 20 (Selecta). After cooling, digested samples were diluted with distilled water to 10 mL in polypropylene tubes, filtered in 0.45 µm filters (#17463443, Scharlab) and kept in polystyrene tubes until determination. For the analysis, 0.5 mL of the sample was diluted to 10 mL with a solution of 2% nitric acid and 1% hydrochloric acid. Silicon determination was performed in an Inductively Coupled Plasma Mass Spectrometer System (ICP-MS) Agilent 7900 in H2 mode, using germanium as internal standard. A calibration curve was also prepared from silicon standard for ICP (#08729, Sigma), and standard solutions were digested and treated the same way as the mice samples. Data are expressed as µg Si/g sample.

Statistical analysis

All the values represent the mean ± SEM of at least three in- dependent experiments except the in vivo experiment with mice, where a single representative experiment is shown. Significance was determined by one-way ANOVA or two-way ANOVA followed by Tukey's post-test, Sidak's post-test, or Student's T-test using GraphPad Prism 8 software. A p-value below 0.05 was considered statistically significant ($*p < 0.05$; $**p < 0.01$; $***p < 0.001$) or ($\#p < 0.05$; $\#\#p < 0.01$; $\#\#\#p < 0.001$). For *in vivo* studies, mice were randomly assigned to treatment groups; the sample size was not pre-determined.

Results

Design, synthesis, and characterization of the communities of nanoparticles

Considering our objective, i.e. to use stigmergy communication concepts to enhance treatment in a mouse model of human triple-negative breast cancer (TNBC) (**Fig. 1**), we prepared two sets of nanodevices using MSNs as inorganic scaffold (**Table S1** and **Fig. S1**). The first nanoparticle is a pro-senescent nanodevice (**NP(palbo) PEG-MUC1**) and is designed for the targeted induction of senescence in TNBC. To prepare this first nanoparticle, the pores of MSNs were loaded with palbociclib (**NP(palbo)**) and functionalized with (3-mercaptopropyl)trimethoxysilane. Then, the thiol groups onto the surface

were reacted first with 2,2'-dipyridyldisulfide and then with a heterobifunctional poly(ethylene glycol) (NHS-PEG-SH) that was finally anchored to the nanoparticles through the formation of disulfide bonds (**NP(palbo)PEG**). Finally, the 5' amino-modified MUC1- binding aptamer (5′ NH_2-GCAGTTGATCCTTTGGATACCCTGG-3') was covalently bonded onto the PEG derivative on the external surface through the formation of amide bonds, yielding the final nanodevice **NP(palbo)PEG-MUC1** (**Fig. 2A**). Mucin 1 (MUC1) is a transmembrane glycoprotein considered as an oncomarker due to its overexpression in breast cancer and other carcinomas.[40–42] Following a similar procedure, nanoparticles **NP(saf)PEG**, **NP(saf)PEG-MUC1** (loaded with safranine O) and **NP(ICG)PEG**, **NP(ICG)PEG-MUC1** (loaded with indocyanine green for in vivo tracking purposes) were also prepared. It is expected these nanoparticles will be internalized selectively by breast cancer cells through MUC1-mediated endocytosis with the subsequent cargo delivery (i.e. palbociclib, safranine O, or ICG) due to the high intracellular concentration of glutathione (GSH) that would reduce the disulfide bonds of the capping PEG in the endocytic compartment.[43] In order to evaluate the targeting ability of the aptamer functionalized nanoparticles, a similar nanodevice loaded with safranine O but functionalized with a random DNA sequence unable to bind with MUC1 receptor (i.e. 5' NH_2-AAGCACTTTCAGTGGGGAGGAGGGTTGATAGGTTAAGAG-3') was also prepared (**NP(saf)PEG-Random**). Besides, another set of nanoparticles without any cargo was synthesized to check the biocompatibility of the inorganic support and the gating ensemble (**NP-PEG**).

The second nanoparticle (**NP(nav)-Gal**) was recently reported by us and we have also described its use in the selective release of entrapped cargos in senescent cells.[26,36–39,44] To prepare **NP(nav)-Gal**, MSNs were loaded with navitoclax and externally functionalized with (3-aminopropyl) trimethoxysilane. Finally, the amino moieties were reacted with a hexa-galacto-oligosaccharide (galactan), yielding the final system (**Fig. 2B**). Following the same procedure, nanoparticles without cargo (**NP-Gal**) or loaded with the dye nile blue and coated with galactan were also prepared (**NP(NB)-Gal**) Once internalized, the high lysosomal β-galactosidase activity in senescent cells induces the hydrolysis of the galactan cap, resulting in pore opening and cargo release.

Both sets of nanoparticles were characterized using standard procedures (see Supporting Information for more details). The mesoporous structure of the final nanoparticles was clearly observed by powder X-ray diffraction (PXRD) (**Fig. S2**). In all cases the (100) reflection in the PXRD patterns is observed indicating that the 2D mesoporous structure was preserved during the pore loading process and functionalization. N_2 adsorption-desorption studies (**Fig. S3**) of the calcined **MSNs** showed a type IV isotherm typical of the mesoporous silica materials and a BET specific surface area of 1158.8 m^2/g. In contrast, the N_2 adsorption-desorption isotherms of the final nanodevices was typical of mesoporous systems with partially filled mesopores with reduced specific surfaces (Table S2). TEM images (**Fig. S4**) show for all nanoparticles a similar reticular spherical geometry with a diameter of ca. 100 nm. Furthermore, TEM- EDX mapping studies for **NP(palbo)PEG-MUC1** (**Fig. 2C**) demonstrated the presence of Si (from the silica scaffold), N (from palbociclib and MUC1-targeting aptamer), S (from disulfide bond in the PEG chain) and P (from MUC1 targeting-aptamer). TEM-EDX map for **NP(nav)-Gal** (**Fig. 2C**) shows the presence of Si (from the silica scaffold), S, F, and Cl (from the loaded navitoclax) and N (from navitoclax and the capping galactan oligosaccharide).

Besides, zeta potential (**Fig. S5**, **Table S3**) and hydrodynamic diameter (Table S3) measurements were also conducted. Calcined **MSNs** presented a zeta potential value of -30.9 ± 0.6 mV that changed to 5.7 ± 0.2 mV after pore loading with palbociclib, functionalization of the external surface with mercaptopropyl moieties and subsequent activation with 2,2'-dipyridyldisulfide. After the addition of NHS-PEG-SH, the zeta potential turns to negative values (-32.0 ± 0.3), becoming more negative (-40.3 ± 1.5 mV) when the MUC1-binding aptamer is anchored to give the final **NP(palbo)PEG- MUC1** nanoparticle. Moreover, the hydrodynamic diameter increased after the loading and functionalization process from 161.7 ± 2.7 nm for the calcined **MSNs** to 199.4 ± 6.3 nm for **NP (palbo)PEG-MUC1**. For **NP(nav)-Gal**, zeta potential changed from the initial -30.9 ± 0.6 value to 4.03 ± 0.3 mV after loading the pores with navitoclax and grafting of galactan. Besides, the hydrodynamic diameter increased from 161.7 ± 2.7 for **MSNs** to 253.4 ± 2.2 nm for **NP(nav)-Gal**. A single population distribution was observed for all the systems suggesting that nanoparticles were not aggregated. Finally, the amount of palbociclib (59 mg/g SiO_2) and PEG (124 mg/g SiO_2) in **NP(palbo)PEG** were determined by thermogravimetric analysis. Besides the amount of palbociclib in **NP(palbo)PEG** was confirmed by delivery studies in the presence of glutathione through UV-Vis spectrum (52.6 mg / g SiO_2) using a calibration curve of palbociclib at increasing concentrations (**Fig. S6**). Thermogravimetric analysis and delivery studies were also used to determine the amount of navitoclax (54 mg/g SiO_2) and galactan (167 mg/g SiO_2) in **NP(nav)-Gal** (Table S4).

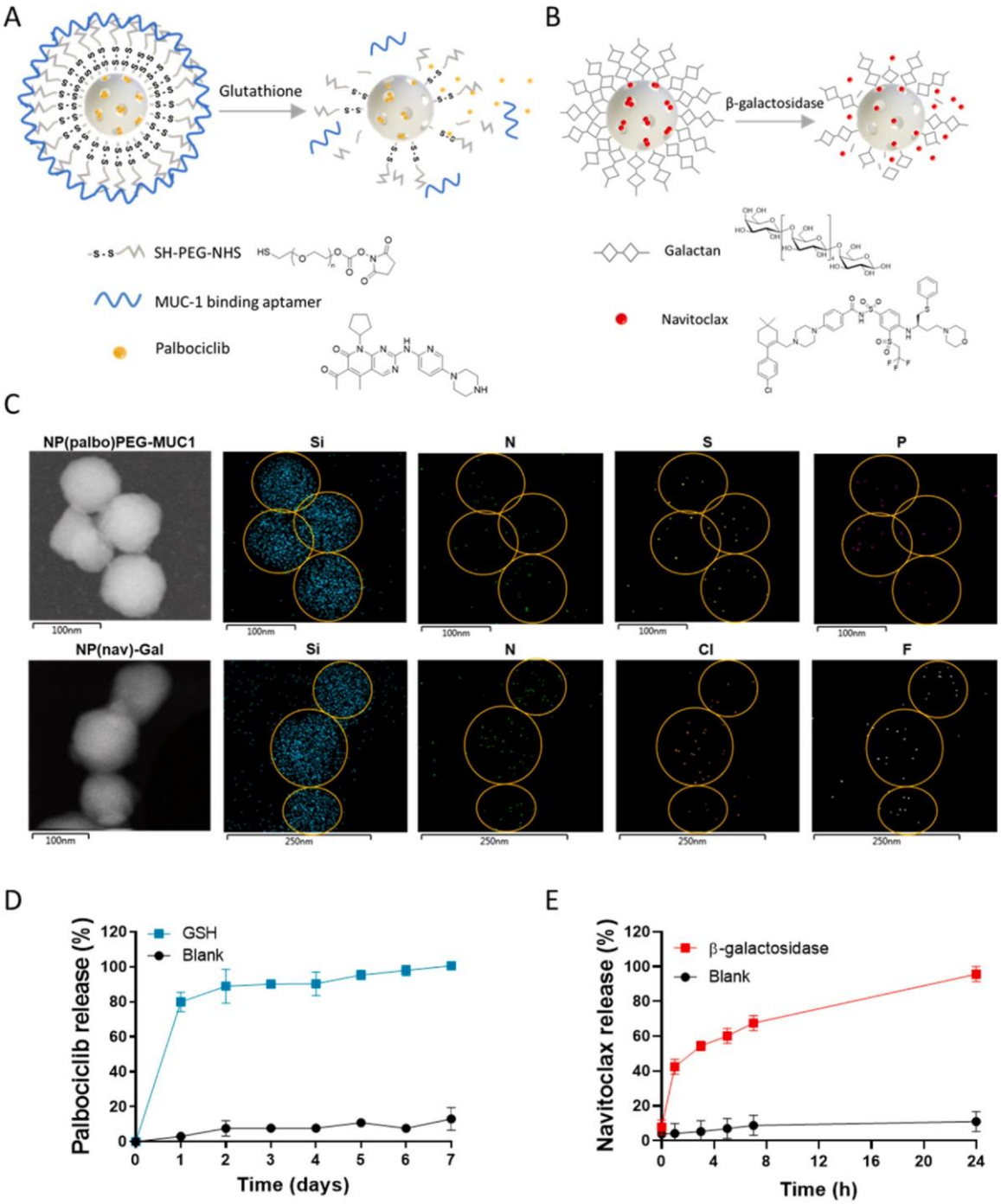

Fig. 2. Nanoparticle design and characterization. (A) Scheme of mesoporous silica nanoparticles (MSNs) loaded with palbociclib and capped with a PEG chain attached to the MUC1-targeting aptamer. (B) Scheme of MSNs loaded with navitoclax and capped with ahexagalacto-oligosaccharide (galactan). (C) TEM-EDX map for **NP(palbo)PEG-MUC1** showing the presence of Si (from the silica scaffold), N (from palbociclib and MUC1-targeting aptamer), S (from the disulfide bond), and P (from MUC1 targeting-aptamer). TEM-EDX map for **NP(nav)-Gal** shows the presence of Si (from the silica scaffold), S, F, and Cl (from the cargo navitoclax) and N (from navitoclax and galactan). (D) Release profile of palbociclib from **NP(palbo)PEG** in the absence (blank, black line) and presence of GSH (blue line) in PBS. Data represent mean ± SEM (n = 3). (E) Release profile of navitoclax from NP(nav)-Gal, in the absence (blank, black line) and presence of β-galactosidase (red line) in water at pH 4.5. Data represent mean ± SD (n = 3).

To study the gating ability of the capping PEG as well as the possibility of sustained release of palbociclib for longer times, cargo delivery from **NP(palbo)PEG** was studied in PBS in the presence or the absence of GSH at different times (**Fig. 2D** and **S7A**). GSH is a tripeptide capable of reducing disulfide bonds and its presence has been used for the controlled release of cargos inside cells, as GSH concentration in cells (10 mM) is significantly higher than in blood plasma (2 μM). [45] As shown in **Fig. 2D** and **S7A**, a negligible palbociclib release was observed (ca. 10% after 120 h) for **NP(palbo)PEG** in the absence of GSH. However, a remarkable delivery was found in the presence of GSH, being almost all the cargo released during the first hour. Similar GSH-triggered cargo delivery was observed for **NP(saf)PEG** and **NP(ICG)PEG**. Slightly differences in the cargo release profile from **NP(palbo)PEG**, **NP(saf)PEG** and **NP(ICG)PEG** can be attributed to chemical

differences and solubility of the cargo molecules in each case (**Fig. S7B** and **S7C**). Overall, our results demonstrated in all cases the proper working of the designed molecular gate with the subsequent controlled release of the cargo only in the presence of the specific stimulus. Besides, **NP(nav)-Gal** displayed a negligible drug delivery in solution, while navitoclax was clearly delivered in the presence of the β-galactosidase enzyme (**Fig. 2E**). [26,37–39] Similar cargo delivery was observed for **NP(NB)Gal** in the presence of the β-galactosidase enzyme (**Fig. S6D**). Finally, the bio- compatibility of the newly prepared nanodevices was assessed. For this purpose, cell viability studies in the presence of **NP-PEG** (without cargo) at different concentrations were performed in MDA- MB-231 breast cancer cells (**Fig. S8A**). After 7 days of treatment, cell viability was kept up to 80% even at the highest **NP-PEG** concentrations (200 μg/mL). We also found that **NP-Gal** was well-tolerated for MDA-MB-231 cell line (**Fig. S8B**) [26,37,38].

Targeted internalization of MUC1-functionalised nanoparticles and induction of senescence in vitro

As described above, the pro-senescent nanodevice (first community of nanoparticles) was functionalized with an aptamer de- signed to target the MUC1 receptor in TNBC MDA-MB-231 cells. MUC1 is a glycoprotein [46,47] that is overexpressed in MDA-MB- 231 cells.[41] The preferential internalization of the nanodevice loaded with safranine O (**NP(saf)PEG-MUC1**) in MDA-MB-231 cells was studied using confocal microscopy and flow cytometry (**Fig. 3**). Confocal images revealed a red emission, ascribed to safranin O, in MDA-MB-231 cells (**Fig. 3A**, left image) after 2 h of treatment with **NP(saf)PEG-MUC1**. To demonstrate the targeting ability of the cap- ping MUC1-binding aptamer, similar cell internalization studies were performed with nanoparticles functionalized with a random DNA sequence (**NP(saf)PEG-Random**). When cells were treated with **NP(saf)PEG-Random**, a much lower safranine O red emission in cells was found (**Fig. 3A**, right image). Quantification of confocal images demonstrated a 3-fold higher safranine O emission in MDA-MB-231 cells treated with **NP(saf)PEG-MUC1**, when compared to those treated with **NP(saf)PEG-Random** (**Fig. 3B**). Besides, the safranin O release from **NP(saf)PEG-MUC1** and **NP(saf)PEG-Random** nanoparticles was monitored using flow cytometry (**Fig. 3C**). The results corroborated the preferential uptake of **NP(saf)PEG-MUC1** by ca. 80% of the cells after 2 h of treatment, compared to ca. 40% of cells treated with **NP(saf)PEG-Random**. These results demonstrate the targeting ability of **NP(saf)PEG-MUC1** to MDA-MB-231 breast cancer cells.

After demonstrating the ability of **NP(saf)PEG-MUC1** to target TNBC cells, we tested if **NP(palbo)PEG-MUC1** was able to induce senescence. For that purpose, MDA-MD-231 cells were treated with 80 μg/mL of **NP(palbo)PEG-MUC1** for 7 days (corresponds to 2.5 μM of free palbociclib). Free palbociclib at 2.5 μM treatment was used as a control of the senescence induction. Cells treated with free palbociclib or with **NP(palbo)PEG-MUC1** have a different morphological appearance when compared with non-treated cells (**Fig. 3D**). Palbociclib-treated cells became larger, flattened, and with higher granularity due to the presence of an expanded lysosomal compartment and are stained in blue when treated with X-Gal due to high activity of β-galactosidase enzyme in senescent cells.[48] The induction of senescence using encapsulated palbociclib in **NP(palbo) PEG-MUC1** was similar to that observed for free palbociclib administration. Besides, western blot assays demonstrated a reduction in the expression of pRb after the treatment with free palbociclib or **NP(palbo)PEG-MUC1** (**Fig. 3E**). The hypo-phosphorylation of pRB protein is a recognized marker of senescence induction as a direct consequence of the inhibition of CDK4/6 proteins after palbociclib treatment, which caused cell cycle arrest in the G1/S transition phase.[49] Besides, there was an up-regulation of the p21 protein when the cells were treated with palbociclib or **NP(palbo)PEG- MUC1**. These results demonstrated that **NP(palbo)PEG-MUC1** in- duces senescence in MDA-MB-231 cells.

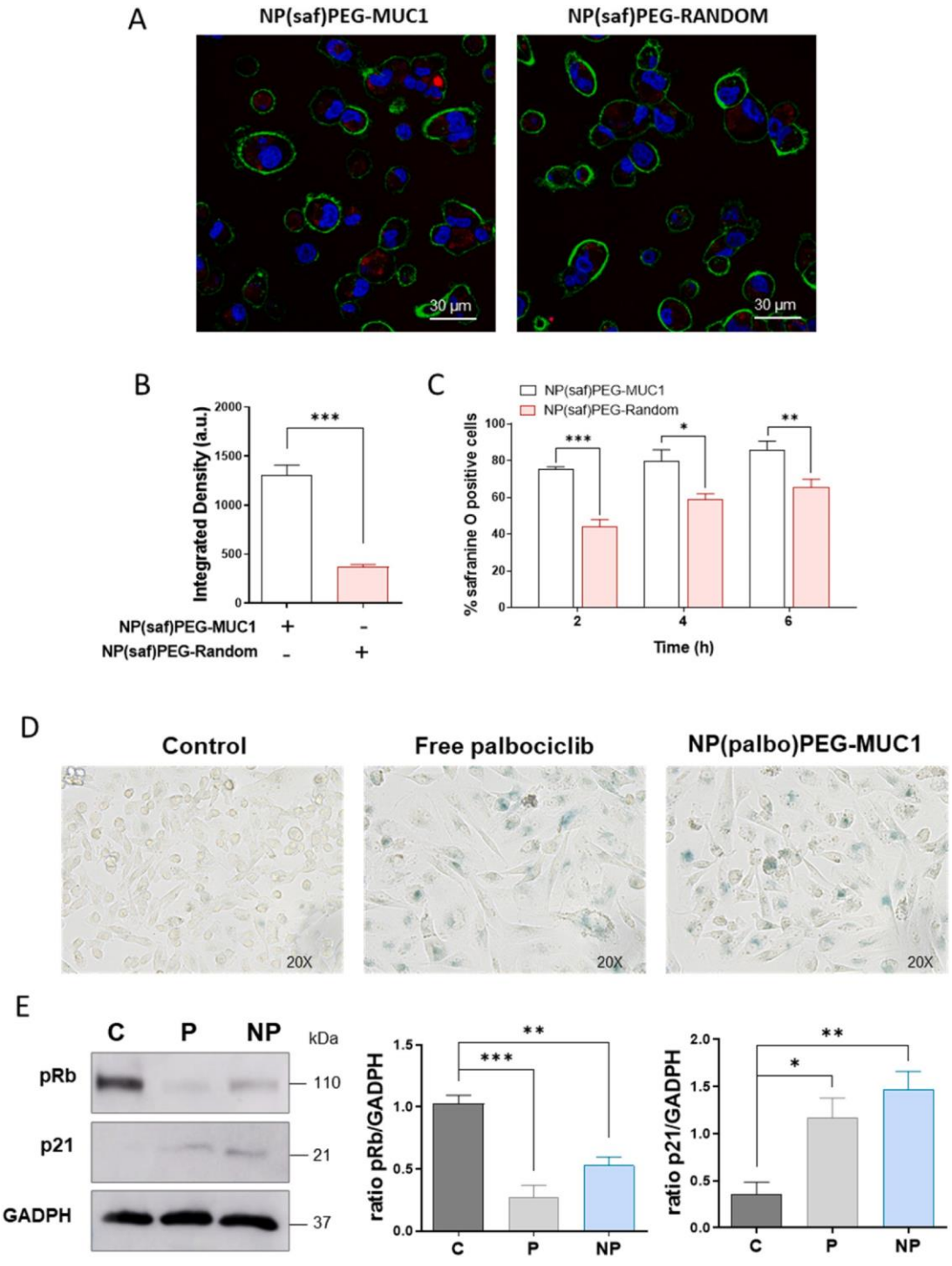

Fig. 3. NP(saf)PEG-MUC1 is preferentially internalized in MDA-MB-231 cells, and NP(palbo)PEG-MUC1 efficiently induces senescence**.** (A) Representative confocal images of **NP (saf)PEG-MUC1** internalization vs **NP(saf)PEG-Random** internalization by MDA-MB-231 cells after 2 h of treatment. Safranine O (red), WGA Alexa 488 (green), and nucleus (blue). (B) Fluorescence intensity quantification of confocal images of **NP(saf)PEG-MUC1** internalization (white bars) vs **NP(saf)PEG-Random** internalization (red bars) by MDA-MB-231 cells after 2 h of treatment. Data represent mean ± SEM (n = 3), and statistical significance was assessed by two-tailed Student's T-test (***p-value < 0.001.) (C) Percentage of safranine O positive MDA-MB-231 cells in flow cytometry after 2, 4 and 6 h of NP(saf)PEG-MUC1 (white bars) and NP(saf**)**PEG-Random (red bars) treatment. Data represent the means ± SEM of at least three independent experiments and statistical significance was assessed by two-way ANOVA followed by Sidak's post-test (*p < 0.05; **p < 0.01; ***p < 0.001) (D) β-Galactosidase staining of proliferating control (C), 2.5 µM free palbociclib-treated (P) MDA-MB-231 cells and 80 µg/mL treated NP(palbo)PEG-MUC1 (NP) treated MDA-MB-231 cells. Senescence induction was confirmed by high β-galactosidase activity (blue color) in free palbociclib or nanoparticle-treated cells at pH 6. (E) Western Blot characterization of proliferating (C), 2.5 µM free palbociclib-treated (P) MDA-MB-231 cells and 80 µg/mL treated NP(palbo)PEG-MUC1 (NP) MDA-MB-231 cells. After pal- bociclib treatment pRb (110 kDa) expression decreases whereas p21 (21 kDa) expression increases. Quantification of the bands using GADPH as a loading control (n ≥ 3) (right panels). Values are expressed as mean ± SEM, and statistical significance was assessed by one-way ANOVA followed by a Tukey post-test: *p < 0.05; * *p < 0.01; * **p < 0.001.

Cooperative behavior by stigmergy: targeted induction of senescence and senolysis in vitro

Once assessed the targeting ability and the pro-senescent capacity of **NP(palbo)PEG-MUC1** in MDA-MB-231 cells, we studied if the proposed stigmergy communication using nanoparticles could be suitable to enhance cancer therapy. In this respect, MDA-MB-231 cells were treated, in a first step, with free palbociclib or **NP(palbo)- PEG-MUC1** and, in a second step, with free navitoclax or **NP(nav)-Gal**. Then cells were incubated for 72 h and cell viability was measured (**Fig. 4A**).

Addition of free navitoclax to free palbociclib-treated MDA-MB-231 cells resulted in a half-maximal inhibitory concentration (IC_{50}) of 2.71 µM (Fig. S9A). Remarkably, a higher senolytic activity was obtained when free palbociclib-treated MDA-MB-231 cells were incubated with **NP(nav)-Gal** nanoparticles (**Fig. 4B**) (IC_{50} value of 1.41 µM). On the other hand, when senescence is first induced by the treatment of MDA-MB-231 cells with **NP(palbo)PEG-MUC1**, treatment with free navitoclax also results senescent cells death (IC_{50} of 6.05 µM) (**Fig. S9A**). Besides, when MDA-MB-231 cells are treated with the two nanodevices (**NP(palbo)-PEG-MUC1** and **NP(nav)-Gal**), a remarkable IC_{50} of 1.56 µM is obtained (**Fig. 4B**). Moreover, the senolytic activity of simultaneous co-treatment with free palbociclib and free navitoclax was evaluated in vitro and any increased effect was observed (**Fig. S9B**). These results suggest a beneficial effect due to the combination of **NP(palbo)-PEG-MUC1** and **NP(nav)-Gal**. The stigmergy strategy using the two nanoparticles effectively results in the specific cell death of senescent cells with an increased therapeutic effect compared to the administration of the free drugs.

We next investigate the death mechanism of both combination of the free drugs and the nanodevices in MDA-MB-231 cells. For that we studied the mitochondria potential (**Fig. 4C**) using the tetramethylrhodamine ethyl ester (TMRE) dye [50,51]. The results revealed that, after free palbociclib or **NP(palbo)-PEG-MUC1** treatment, navitoclax treatment, as a free drug or encapsulated in **NP (nav)-Gal**, decreased the mitochondrial membrane potential to ca. 60%, indicating apoptosis triggering. Altogether, these results corroborate the potential of the stigmergy paradigm by using a first community of **NP(palbo)PEG-MUC1** nanoparticles to transform tumor cells in senescent cells in combination with a second community of **NP(nav)-Gal** nanoparticles to eliminate senescent cancer cells.

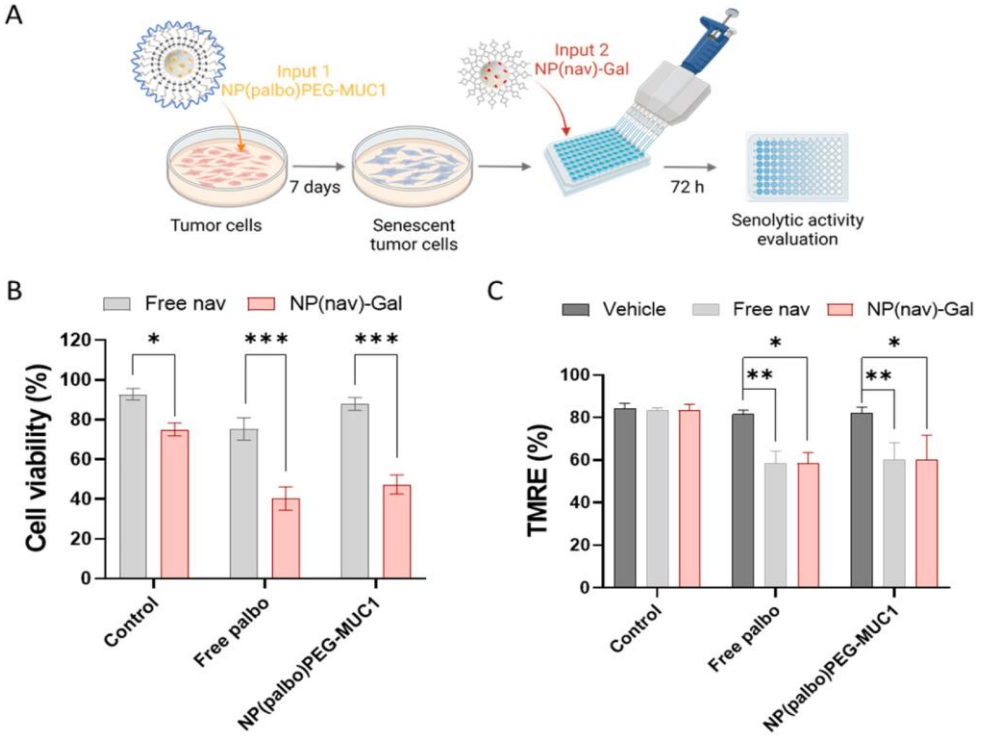

IC50 (µM)	Free palbo	NP(palbo)PEG-MUC1
Free nav	2.71	6.05
NP(nav)-Gal	1.41	1.56

Fig. 4. Cytotoxicity profile of the combination of free palbociclib or **NP(palbo)PEG-MUC1** with free navitoclax or **NP(nav)-Gal** in MDA-MB-231 cells. (A) Scheme of cell viability assays to evaluate the communication system. (B) Cell viability after 72 h of treatment at 0.16 µM and the IC_{50} values determined for each combined treatment. Control stands for proliferating MDA-MB-231 cells (C) Mitochondrial polarization status in the above-described conditions. Control stands for proliferating MDA-MB-231 cells. Vehicle is 1% DMSO. Data represent the means ± SEM of at least three independent experiments. Statistical significance was determined by two-way ANOVA followed by Tukey post-test (*$p < 0.05$; **$p < 0.01$; ***$p < 0.005$).

Stigmergic communication by targeted induction of senescence and senolysis using nanoparticles in vivo in TNBC MDA-

MB-231 xenografts

As stated above, stigmergy is a communication method in which individuals (in our case, nanoparticles) communicate with each other by changing the surrounding. The results above demonstrate *in vitro* that a first community of nanoparticles is able to transform tumor cells in senescent cells in combination with a second community of nanoparticles that eliminate senescent cells selectively. However, a most appealing issue of stigmergic communication is its high potential to be applied in highly complex system such as an in vivo environment.

To this aim we first evaluated nanoparticles' ability to target breast cancer tumors *in vivo*. For this purpose, we tracked the activity of the two sets of nanoparticles loaded with fluorescent reporters (i.e. **NP(ICG)PEG-MUC1** and **NP(NB)-Gal**). For that, Balb/c nude female mice were injected on mammary pads with TNBC MDA-MB-231 cells. When tumors volume reached 220 mm^3, **NP(ICG)PEG-MUC1** nanoparticles were intraperitoneally administrated (**Fig. 5A**). *Ex vivo* imaging studies of ICG distribution at 24 h post-injection demonstrated the accumulation of the **NP(ICG)PEG-MUC1** in MDA-MB-231 tumors with the subsequent release of ICG (**Figs. 5B** and **C**).

In an additional experiment, we evaluated if **NP(NB)-Gal** are able to target senescent tumors induced by the action of the first community of **NP(palbo)PEG-MUC1** nanoparticles. Thus, after two weeks of treatment with **NP(palbo)PEG-MUC1**, **NP(NB)-Gal** were intraperitoneally administered (**Fig. 5D**). IVIS imaging studies at 24 h post-injection shows the preferential release of the loaded of nile blue fluorophore in MDA-MB-231 senescent tumors *ex vivo* (**Figs. 5E** and **5F**) and *in vivo* (**Fig. 5G**). These experiments demonstrated that (i) **NP(ICG)PEG-MUC1** targets MDA-MB-231 tumors and (ii) treatment first with the palbociclib-loaded nanoparticles **NP(palbo)PEG-MUC1** allows tumor targeting by the second **NP(NB)-Gal** nano-particles.

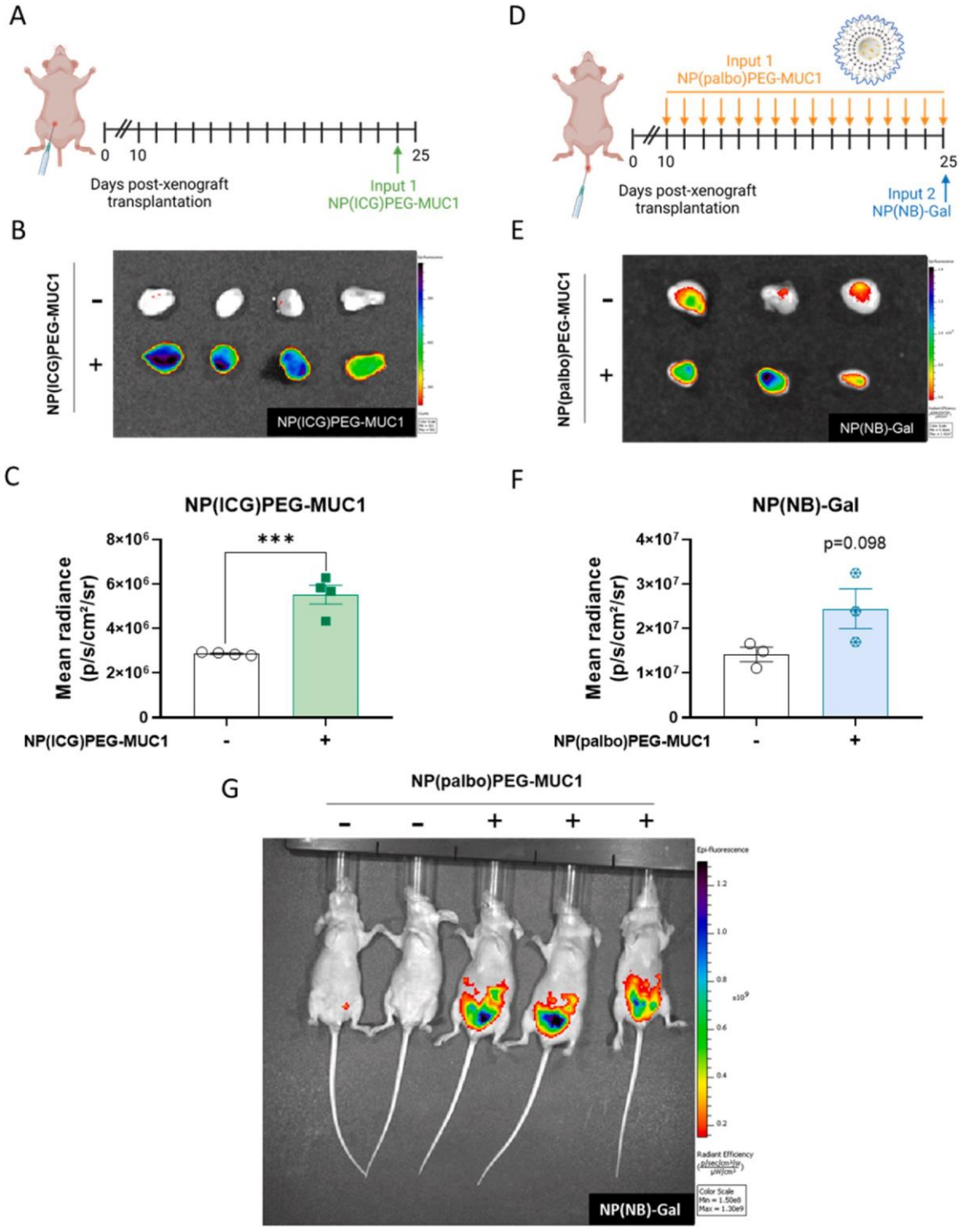

Fig. 5. **NP(ICG)PEG-MUC1** nanoparticles selectively release their cargo in the tumors of TNBC model mice, and **NP(NB)-Gal** nanoparticles selectively release their cargo in the senescent tumors. (A) Balb/c nude female mice were injected on mammary pads with TNBC MDA-MB-231 cells. When tumors volume reached 220 mm^3 (day 24), **NP(ICG)PEG-MUC1** nanoparticles (i.p.) were administered and IVIS imaging was performed. (B) *Ex vivo* IVIS spectrum imaging of tumors 24 h post-injection of **NP(ICG)PEG-MUC1** and (C) fluorescence quantification by Living Image® 4.3.1 software. Data represent mean ± SEM (n = 4), and statistical significance was assessed by two-tailed Student's T-test (***p- value < 0.001) (D) Balb/c nude female mice were injected on mammary pads with TNBC MDA-MB-231 cells. When tumors volume reached 60 mm^3 (day 10), palbociclib treatment started (encapsulated in **NP(palbo)PEG-MUC1** nanoparticles (i.p.)) and was maintained daily for 15 days. On day 25, **NP(NB)-Gal** nanoparticles (i.p.) were administered and IVIS imaging was performed. (E) *Ex vivo* IVIS spectrum imaging of senescent tumors 24 h post-injection of **NP(NB)-Gal** and (F) fluorescence quantification by Living Image® 4.3.1 software. Data represent mean ± SEM (n = 3), and statistical significance was assessed by two-tailed Student's T-test (*p-value < 0.05) (G) *In vivo* imaging studies by IVIS of **NP(NB)-Gal** distribution after 24 h post-injection in MDA-MB-231 bearing mice previously treated with vehicle (as a control) or **NP(palbo)PEG-MUC1** to induce senescence in tumors.

Finally, to validate the proposed therapeutic stigmergic communication, senescence-inducing chemotherapy with

NP(palbo)- PEG-MUC1 in combination with the senolytic **NP(nav)-Gal** was tested *in vivo*. MDA-MB-231 cells were injected subcutaneously in the second lower right breast of nude BALB/C mice. When tumor volume reached an average of 60 mm^3, daily therapy was initiated with either vehicle (sodium lactate), 5 mg/kg palbociclib (via oral gavage), or **NP(palbo)PEG-MUC1** (via i.p. injection at equivalent palbociclib dose) (**Fig. 6A**). As a result of palbociclib treatment, a significant decrease in tumor growth was observed in mice treated with monotherapy of either free palbociclib or **NP(palbo)PEG-MUC1** (**Fig. 6B**). Besides, X-Gal staining showed the overexpression of β-galactosidase in tumor slides of mice treated with either free palbociclib or **NP(palbo)PEG-MUC1** (**Fig. 6 C**), indicative of the transformation of the environment, from tumors to senescent tumors. Cell senescence induction in tumors was also assessed by immuno-histochemical staining of the proliferation biomarker Ki67 in tumor autopsy samples and by the increase in p53 positive cells (**Fig. 6 C** and **Fig. S10**). All these results confirmed the suitability of **NP(palbo)- PEG-MUC1** nanoparticles for senescence induction in animal models.

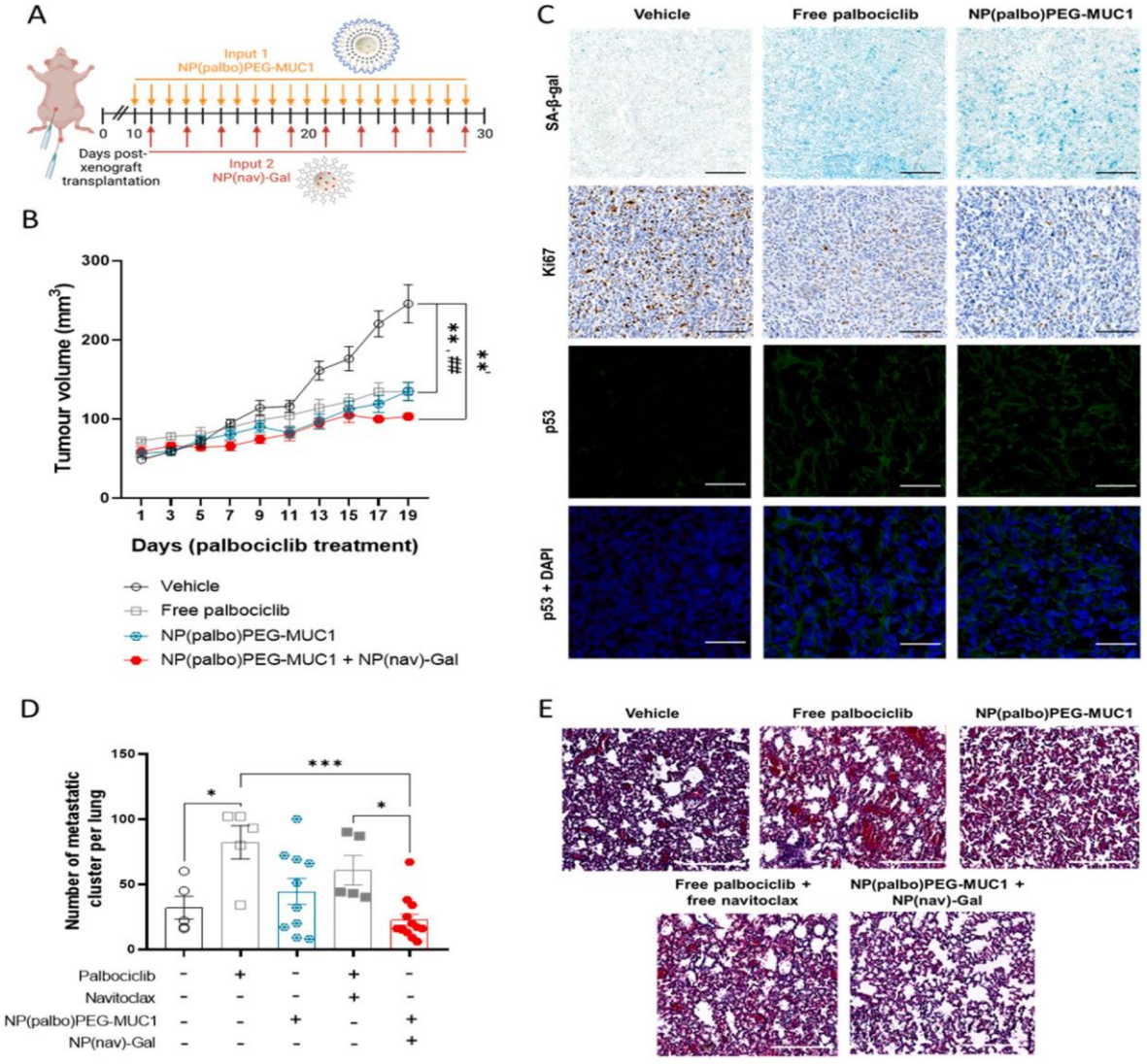

Fig. 6. *In vivo* evaluation of communication by stigmergy using **NP(palbo)PEG-MUC1** and **NP(nav)-Gal** in TNBC**.** (A) Balb/c nude female mice were orthotopically injected with TNBC MDA-MB-231 cells and treated daily with either vehicle or free palbociclib or **NP(palbo)PEG-MUC1**. $2{\cdot}10^6$ MDA-MB-231 cells were subcutaneously implanted on mammary pads. When tumors volume reached 60 mm^3, palbociclib treatment started (encapsulated in nanoparticles or as a free drug) and was maintained daily for 19 days. **NP(nav)-Gal** daily treatment started one day after free palbociclib or **NP(palbo)PEG-MUC1** treatment. (B) Tumor volume (mm^3) for the different treatments. Vehicle stands for 50 mM sodium lactate pH 4.5 (o.g.) and DMEM medium (i.p and i.v.). Statistical analysis was carried out using GraphPad Prism 8, and results were compared by one-way ANOVA followed by Tukey's post-test (*Vehicle vs free palbociclib; #vehicle vs **NP(palbo)PEG-MUC1**; * *' vehicle vs **NP(palbo)PEG-MUC1** + **NP(nav)-Gal**) (*$p < 0.05$; **$p < 0.01$; ***$p < 0.001$). Data represent the mean ± SEM ($n \geq 5$). (C) Photograph of representative tumor sections stained with X-gal, immunostained with Ki67 and p53. Scale bar, 200 µm. (D) Quantification of metastatic lung clusters found in lung sections taken from xenograft MDA-MB-231 tumor-bearing mice or different treatments. (E) Representative tissues images were micro- scopically counted. Statistical analysis was carried out using GraphPad Prism 8, and results were compared by one-way ANOVA followed by Tukey's post-test (*$p < 0.05$; **$p < 0.01$; ***$p < 0.001$). Data represent the mean ± SEM ($n \geq 5$). E) H&E staining of representative metastatic lungs clusters. Scale bar, 500 µm.

In a second step, the effect of the second swarm of nanoparticles **NP(nav)-Gal** was evaluated. Thus, one day after **NP(palbo)PEG-MUC1** administration, senolytic treatment was initiated with **NP(nav)-Gal**. Remarkably, concomitant treatment with **NP(palbo)PEG- MUC1** plus **NP(nav)-Gal** resulted in a significant reduction of tumor growth (**Fig. 6B** and **Fig. S11**). The results confirmed the proper achievement of therapeutic communication using two sets of nanoparticles that act cooperatively. The modification of cancer cells into senescent cells induced by **NP(palbo)PEG-MUC1** (modifying the environment) allows the second community of nanoparticles (**NP(nav)-Gal**) to deliver the senolytic cargo in senescent cells, resulting in a significant reduction in tumor size. Besides, a similar tumor reduction in mice treated with an equivalent concentration of free palbociclib and free navitoclax was found. However, a remarkable reduction of drug side effects was observed when animals were treated with the encapsulated drugs (vide infra).

Attending to the metastatic profile of TNBC tumors, we also evaluated lung metastasis in the mice bearing MDA-MB-231 tumors. Metastatic cell clusters were found in lung sections of MDA-MB-231 xenograft mice (**Figs. 6D** and **6E**). After free palbociclib treatment, a significant increase in the number of metastatic clusters in lungs is detected. In contrast, a significant decrease was found in those animals co-treated with **NP(palbo)PEG-MUC1** and **NP(nav)-Gal** (**Figs. 6D** and **6E**). Histological examination of apoptosis through TUNEL assay in tumor slides evidenced that senescent cells undergo apoptosis after treatment with either free palbociclib plus free navitoclax or **NP(palbo)PEG-MUC1** plus **NP(nav)-Gal**. Moreover, the combinational treatment with the nanoparticles revealed the highest TUNEL signal (**Fig. 7A** and **7B**). To study the safety of the stigmergy strategy using **NP(palbo)PEG-MUC1** plus **NP(nav)-Gal** nanoparticles for two weeks of sustained treatment, biochemistry analyses were performed to evaluate hepatic and liver function (**Fig. S12**). Besides, to discard a potential pro-inflammatory effect of the nanoparticles, the levels of neutrophils, lymphocytes, and monocytes were analyzed in blood samples (**Fig. S13**). No significant differences between animals un-treated or treated with nanoparticles were observed. In conclusion, **NP(palbo)PEG-MUC1** plus **NP(nav)-Gal** treatment does not induce any toxicity or side effects derived from two weeks of sustained nanoparticles administration.

Moreover, biodistribution studies were carried out by de- termining Si levels in various organs (lung, liver, spleen, kidneys) and tumors by inductively coupled plasma mass spectroscopy (ICP-MS) (Fig. S14). The levels of Si detected indicated that nanoparticles reached the tumors. Besides, Si was also detected in organs asso- ciated with nanoparticle elimination. Thus, in the case of **NP(palbo) PEG-MUC1,** Si was observed in the spleen and kidneys, suggestingrenal clearance.[52] In contrast, when **NP(nav)-Gal** was added to the treatment, Si content was also observed in the liver, thus suggesting a combined hepatobiliary clearance with renal excretion.[53,54].

Regarding the use of palbociclib and navitoclax, we also noticed that encapsulation improves the therapeutic profile of these drugs. Palbociclib and navitoclax are usually given orally dissolved in sodium lactate or 15% DMSO/85% PEG400, respectively, to facilitate their solubility and thus administration.[37,38,55] The use of nanoparticles encapsulating these drugs allows the preparation of water-soluble suspensions, such as PBS or DMEM, facilitating their administration by other different routes widely used for parenteral administration (such as i.v. and i.p) [56–58]. Besides the encapsulation remarkably minimized undesired drug side effects. Treatment with free palbociclib in monotherapy or concomitant treatment of free palbociclib plus free navitoclax reduces animal weight (**Fig. S15**). Besides, the systemic administration of free palbociclib induces senescence not only in tumors, yet it has also been reported that it can induce senescence in veins and thus favor metastasis [26]. In contrast, palbociclib encapsulated in the nanoparticle (**NP(palbo)PEG-MUC1**) significantly reduces mice weight loss, in agreement with a targeted delivery of palbociclib in TNBC tumors compared to the systemic administration. Moreover, encapsulation of palbociclib also resulted in a decrease in metastasis in lungs (see **Fig. 6C**). In addition, the combined treatment **NP(palbo)PEG-MUC1** plus **NP(nav)-Gal** resulted in a significant decrease in metastasis compared to free drugs. The reduction of lung metastasis after **NP(palbo)PEG-MUC1** plus **NP(nav)-Gal** treatment is relevant as metastasis has a significant role in the clinical management of TNBC. Currently, approximately 25% of TNBC patients relapse with distant metastasis [59]. The reduction of the metastatic lung clusters found in this work provide strong support for the potential translation of this strategy involving palbociclib treatments together with navitoclax in hTNBC tumors. It is also noteworthy that the targeted delivery of navitoclax specifically in senescent cells has been reported to reduce off-target effects and platelet toxicity significantly [38,55].

Collectively, these results exhibited the effectiveness of the stigmergy strategy of communication using nanoparticles, con- firming that this principle could be applied in vivo enhancing therapy in tumors. Targeted pro-senescent and senolytic therapies with both nanosystems have shown their benefits in treating TNBC as effectively reduce tumor growth and metastasis and minimize undesired side effects.

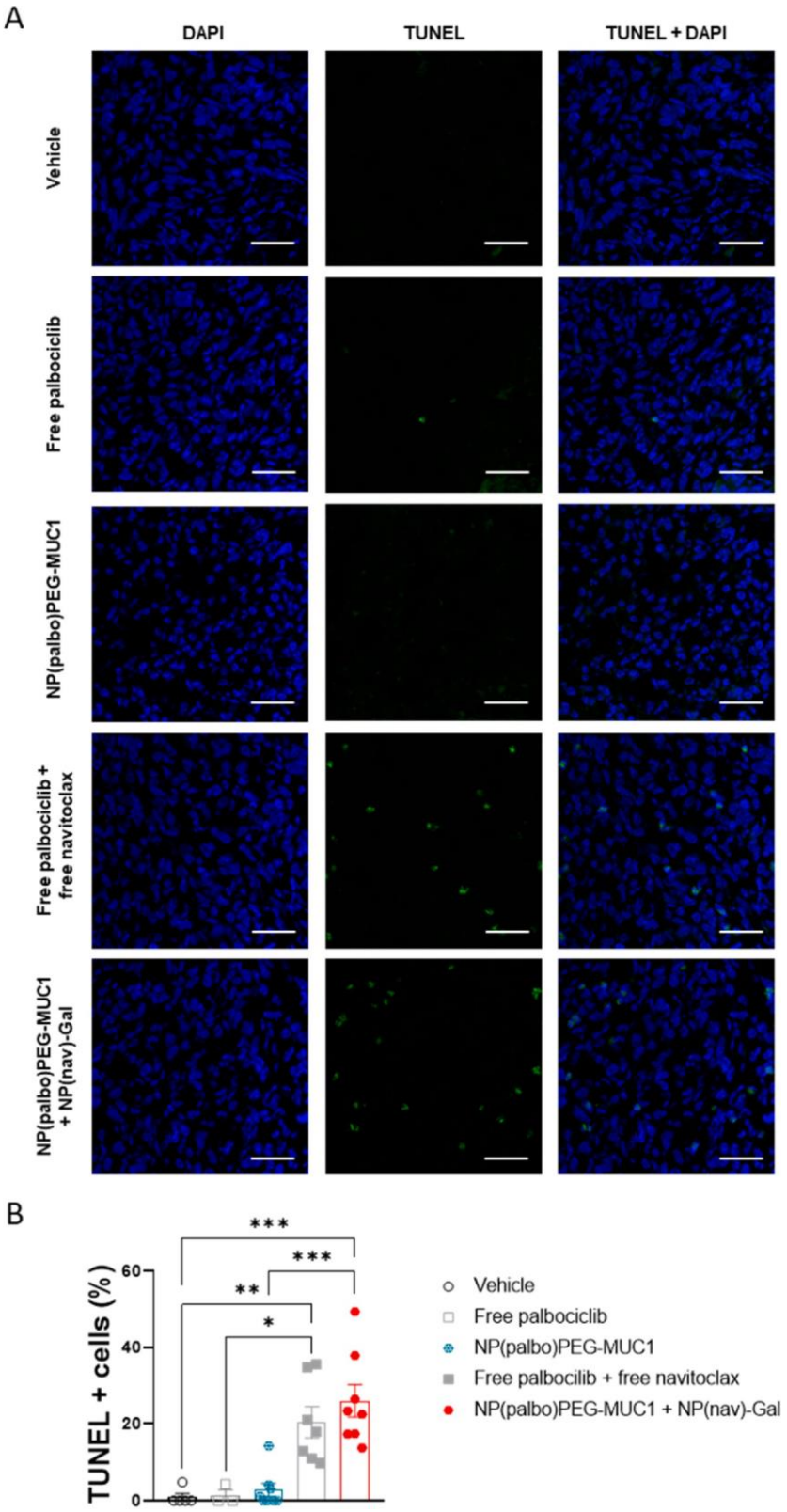

Fig. 7. Histological analysis of apoptosis in tumor slides after treatment. (A) Representative confocal images of TUNEL assay of tumor sections from animals treated with vehicle, free palbociclib, **NP(palbo)PEG-MUC1**, palbociclib + navitoclax and **NP(palbo)PEG-MUC1** + **NP(nav)-Gal** ($n \geq 5$ tumors per group). TUNEL assay was used to confirm the induction of apoptosis in treated and untreated tumor tissues. Vehicle stands for 50 mM sodium lactate pH 4.5 (o.g.) and DMEM medium (i.p and i.v.). Scale bar, 20 µm. (B) Percentage of TUNEL-positive cells in tumors. Quantification was performed in a total of 3 fields per tumor, covering most of the whole tumor section. Data represent the mean ± SEM ($n \geq 5$) and statistical significance was assessed by one-way ANOVA followed by Tukey's post-test (*$p < 0.05$; **$p < 0.01$; ***$p < 0.001$).

Discussion and conclusion

Senescence is a process of cell-cycle arrest that has a crucial role in aging, development, and antitumor response [21,60]. The induction of senescence is a therapeutic approach used in clinical practice to stop tumor progression. Palbociclib (palbo), a CDK4/6 cell-cycle inhibitor, has shown efficacy in treating advanced breast cancer [29,61–64]. However, an unmet medical need appears with the development of drugs that selectively induce senescence, as the presence of senescent cells in tissues is a double-edged sword [65] due to their secretory phenotype that has a negative impact in the tissue microenvironment, triggering tissue dysfunction and/or unfavorable outcomes [66]. In this scenario, senolysis (the selective induction of apoptosis in senescent cells) has been demonstrated to eliminate the adverse side effects of senescent cell accumulation [67,68].

To enhance the therapeutic effect of nanoparticles targeting tumors and to reduce secondary effects, we envisioned the design of a nanoparticle-cell-nanoparticle system that communicates by stigmergy for cancer treatment. The first set of nanoparticles is loaded with palbociclib and capped with a poly (ethylene glycol) covalently linked to a MUC1-binding aptamer (**NP(palbo)PEG-MUC1**). The uptake of **NP(palbo)PEG-MUC1** by triple-negative breast cancer MDA-MB-231 cells is enhanced by the overexpression of MUC1 that facilitates the internalization of the nanoparticles. Treatment with **NP(palbo)PEG-MUC1** induces senescence in the tumor, demonstrated by the stain of tumor slides with X-Gal and by the increase of the expression levels of Ki67 and p53 makers. **NP(palbo)PEG-MUC1** is able to transform the environment in the tumor by inducing senescence, making possible the action of a second community of nanoparticles (**NP(nav)-Gal**) which are loaded with navitoclax and capped with a hexagalactooligosaccharide (galactan). As a consequence of the cooperation by stigmergy, tumor growth reduction, drop of metastases and diminution of drug side effects is observed in in the TNBC mice model

In this work, we demonstrate the high potential of stigmergy communication strategies involving two communities of nanoparticles. The stigmergy protocol enhances the performance of the nanoparticles, allowing them to be applied in targeted transport and drug delivery, opening up new possibilities for cooperative behaviors. Following this stigmergy communication concept, which involves changes in the environment resulting in cooperation between nanoparticles without any need for planning, simultaneous presence, or mutual awareness between the involved systems, a number of plausible networks aimed at increasing drug efficacy and reducing dosages, side effects, and resistance can be envisioned. Communication at the nanoscale by stigmergy can be useful to develop swarm nanoparticles able to interact with their neighbors and local environment, allowing getting functionalities able to cause a deep impact in the way we treat diseases.

Authors' contributions

A.E.-F. performed most of the experiments and contributed to the experimental design, data analysis, discussion and writing. A.G.-F. helped with in vivo experiments, data analysis, discussion, and writing. A.L.-V. helped with in vitro and in vivo experiments, data analysis and discussion. A.M-A synthetized and characterized **NP (nav)-Gal** and performed TEM-EDX images. J.F.B. synthetized and characterized **NP(NB)-Gal**. J.J.E-M helped with in vitro experiments. V.C.-N. helped with the synthetic protocol of **NP(palbo)PEG-MUC1**. G.V.-L. helped with the targeting assays of **NP(palbo)PEG-MUC1**. M.O. supervised the biological studies and contributed to discussion and writing. R.M.-M. and F.S. designed the study and supervised the chemical synthesis and contributed to discussion and writing. All authors revised and commented on the manuscript.

Data Availability

The data that support the findings of this study are available from the corresponding author upon reasonable request.

Declaration of Competing Interest

Pfizer provided palbociclib for the synthesis of **NP(palbo)PEG-MUC1**. The funders had no role in the design, data collection, decision to publish, or preparation of the manuscript and the authors declare that they have no known competing financial interests or personal relationships that could have appeared to influence the work reported in this paper.

Acknowledgments

R.M. laboratory members thank the financial support from the Spanish Government projects RTI2018-100910-B-C41 and RTI2018- 101599-B-C22 and (MCUI/FEDER, EU) and the Generalitat Valenciana (project PROMETEO 2018/024). This work was funded by the European Union. Views and opinions expressed are however those of the author(s) only and do not necessarily reflect those of the European Union or European Research Council. Neither the European Union nor the granting authority can be held responsible for them. This work was supported by the European Research Council (ERC) via Advanced Grant (101052997, EDISON). M.O. thanks the financial support from the Spanish Government project (PID2020-115048RB-I00) and the Generalitat Valenciana (project PROMETEO/2019/065). A.E-F. is grateful to the Spanish Government for her Ph.D. grant (FPU17/05454), A.L-V. is grateful to the Instituto de Salud Carlos III for her Ph.D. i-PFIS

grant (IFI17/00039). J.B. thanks to the Instituto de Salud Carlos III for his Sara Borrell contract (CD19/ 00038). The funders had no role in the design, data collection, de- cision to publish, or preparation of the manuscript. The authors thank Alberto Hernández for the confocal microscope, Alicia Martinez for flow cytometry and Viviana Bisbal for veterinary a ssistance. The authors thank for the use of Biorender.com.

References

[1] X. Zhang, L. Chen, K.H. Lim, S. Gonuguntla, K.W. Lim, D. Pranantyo, W.P. Yong, W.J.T. Yam, Z. Low, W.J. Teo, H.P. Nien, Q.W. Loh, S. Soh, The pathway to intelligence: using stimuli-responsive materials as building blocks for constructing smart and functional systems, Adv. Mater. 31 (2019), https://doi.org/10.1002/ ADMA.201804540

[2] B. de Luis, A. Llopis-Lorente, F. Sancenón, R. Martínez-Máñez, Engineering che- mical communication between micro/nanosystems, Chem. Soc. Rev. 50 (2021) 8829–8856, https://doi.org/10.1039/d0cs01048k

[3] I.F. Akyildiz, F. Brunetti, C. Blázquez, Nanonetworks: A new communication paradigm, (2008). https://doi.org/10.1016/j.comnet.2008.04.001.

[4] B. de Luis, Á. Morellá-Aucejo, A. Llopis-Lorente, T.M. Godoy-Reyes, R. Villalonga, E. Aznar, F. Sancenón, R. Martínez-Máñez, A chemical circular communication network at the nanoscale, Chem. Sci. 12 (2021) 1551–1559, https://doi.org/10. 1039/d0sc04743k

[5] A. Llopis-Lorente, B. de Luis, A. García-Fernández, S. Jimenez-Falcao, M. Orzáez, F. Sancenón, R. Villalonga, R. Martínez-Máñez, Hybrid mesoporous nanocarriers act by processing logic tasks: toward the design of nanobots capable of reading information from the environment, ACS Appl. Mater. Interfaces 10 (2018) 26494–26500, https://doi.org/10.1021/acsami.8b05920

[6] B. de Luis, A. Llopis-Lorente, P. Rincón, J. Gadea, F. Sancenón, E. Aznar, R. Villalonga, J.R. Murguía, R. Martínez-Máñez, An interactive model of com- munication between abiotic nanodevices and microorganisms, Angew. Chem. Int. Ed. 58 (2019) 14986–14990, https://doi.org/10.1002/anie.201908867

[7] C. Giménez, E. Climent, E. Aznar, R. Martínez-Máñez, F. Sancenón, M.D. Marcos, P. Amorós, K. Rurack, Towards chemical communication between gated nano- particles, Angew. Chem. Int. Ed. Engl. 53 (2014) 12629–12633, https://doi.org/10. 1002/anie.201405580

[8] B. de Luis, Á. Morellá-Aucejo, A. Llopis-Lorente, J. Martínez-Latorre, F. Sancenón, C. López, J.R. Murguía, R. Martínez-Máñez, Nanoprogrammed cross-kingdom communication between living microorganisms, Nano Lett. 22 (2022) 1836–1844, https://doi.org/10.1021/acs.nanolett.1c02435

[9] B.C. Buddingh', J. Elzinga, J.C.M. van Hest, Intercellular communication between artificial cells by allosteric amplification of a molecular signal, Nat. Commun. 111 (2020) (2020) 1–10, https://doi.org/10.1038/s41467-020-15482-8

[10] P. Wen, X. Liu, L. Wang, M. Li, Y. Huang, X. Huang, S. Mann, Coordinated mem- brane fusion of proteinosomes by contact-induced hydrogel self-healing, Small 13 (2017), https://doi.org/10.1002/SMLL.201700467

[11] Y. Qiao, M. Li, R. Booth, S. Mann, Predatory behaviour in synthetic protocell communities, Nat. Chem. 9 (2017) 110–119, https://doi.org/10.1038/NCHEM.2617

[12] E. Dubuc, P.A. Pieters, A.J. van der Linden, J.C. van Hest, W.T. Huck, T.F. de Greef, Cell-free microcompartmentalised transcription-translation for the prototyping of synthetic communication networks, Curr. Opin. Biotechnol. 58 (2019) 72–80, https://doi.org/10.1016/J.COPBIO.2018.10.006

[13] E. Bonabeau, M. Dorigo, G. Theraulaz, Swarm, Intell.: Nat. Artif. Syst. (1999), https://doi.org/10.1086/393972

[14] G. Theraulaz, E. Bonabeau, A brief history of stigmergy, Artif. Life 5 (1999) 97–116, https://doi.org/10.1162/106454699568700

[15] J. Werfel, K. Petersen, R. Nagpal, Designing collective behavior in a termite-in- spired robot construction team, Science 343 (2014) 754–758, https://doi.org/10. 1126/science.1245842

[16] J.H. Park, G. Von Maltzahn, M.J. Xu, V. Fogal, V.R. Kotamraju, E. Ruoslahti, S.N. Bhatia, M.J. Sailor, Cooperative nanomaterial system to sensitize, target, and treat tumors, Proc. Natl. Acad. Sci. U. S. A 107 (2010) 981–986, https://doi.org/10. 1073/pnas.0909565107

[17] A.F. Bagley, S. Hill, G.S. Rogers, S.N. Bhatia, Plasmonic photothermal heating of intraperitoneal tumors through the use of an implanted near-infrared source, ACS Nano 7 (2013) 8089–8097, https://doi.org/10.1021/NN4033757

[18] A. Llopis-Lorente, B. Lozano-Torres, A. Bernardos, R. Martínez-Máñez, F. Sancenón, Mesoporous silica materials for controlled delivery based on en- zymes, J. Mater. Chem. B 5 (2017) 3069–3083, https://doi.org/10.1039/ C7TB00348J

[19] B. De Luis, A. García-Fernández, A. Llopis-Lorente, R. Villalonga, F. Sancenón, R. Martínez-Máñez, A 1-to-2 demultiplexer hybrid nanocarrier for cargo delivery and activation, Chem. Commun. 56 (2020) 9974–9977, https://doi.org/10.1039/ d0cc03803b

[20] R. Sager, Senescence as a mode of tumor suppression, Environ. Health Perspect. 93 (1991) 59, https://doi.org/10.1289/EHP.919359

[21] J. Campisi, Cellular senescence as a tumor-suppressor mechanism, Trends Cell Biol. 11 (2001) 27–31, https://doi.org/10.1016/S0962-8924(01)02151-1

[22] M. Collado, M. Serrano, Senescence in tumours: evidence from mice and hu- mans, Nat. Rev. Cancer 10 (2010) 51–57, https://doi.org/10.1038/NRC2772

[23] M. Milanovic, Y. Yu, C.A. Schmitt, The senescence–stemness alliance – a cancer- hijacked regeneration principle, Trends Cell Biol. 28 (2018) 1049–1061, https:// doi.org/10.1016/j.tcb.2018.09.001

[24] T. Saleh, V.J. Carpenter, L. Tyutyunyk-Massey, G. Murray, J.D. Leverson, A.J. Souers, M.R. Alotaibi, A.C. Faber, J. Reed, H. Harada, D.A. Gewirtz, Clearance of therapy-induced senescent tumor cells by the senolytic ABT-263 via interference with BCL-XL–BAX interaction, Mol. Oncol. 14 (2020) 2504–2519, https://doi.org/ 10.1002/1878-0261.12761

[25] T. Saleh, L. Tyutyunyk-Massey, G.F. Murray, M.R. Alotaibi, A.S. Kawale, Z. Elsayed, S.C. Henderson, V. Yakovlev, L.W. Elmore, A. Toor, H. Harada, J. Reed, J.W. Landry, D.A. Gewirtz, Tumor cell escape from therapy-induced senescence, Biochem. Pharmacol. 162 (2019) 202–212, https://doi.org/10.1016/j.bcp.2018.12.013

[26] A. Estepa-Fernández, M. Alfonso, Á. Morellá-Aucejo, A. García-Fernández, A. Lérida-Viso, B. Lozano-Torres, I. Galiana, P.M. Soriano-Teruel, F. Sancenón, M. Orzáez, R. Martínez-Máñez, Senolysis reduces senescence in veins and cancer cell migration, Adv. Ther. 4 (2021) 2100149, https://doi.org/10.1002/adtp.202100149

[27] M. Demaria, M.N. O'Leary, J. Chang, L. Shao, S. Liu, F. Alimirah, K. Koenig, C. Le, N. Mitin, A.M. Deal, S. Alston, E.C. Academia, S. Kilmarx, A. Valdovinos, B. Wang, A. de Bruin, B.K. Kennedy, S. Melov, D. Zhou, N.E. Sharpless, H. Muss, J. Campisi, Cellular senescence promotes adverse effects of chemotherapy and cancer relapse, Cancer Disco 7 (2017) 165–176 https://doi.org/10.1158/2159-8290.CD-16-0241.

[28] S. Wedam, L. Fashoyin-Aje, E. Bloomquist, S. Tang, R. Sridhara, K.B. Goldberg, M.R. Theoret, L. Amiri-Kordestani, R. Pazdur, J.A. Beaver, FDA approval summary: palbociclib for male patients with metastatic breast cancer, Clin. Cancer Res 26 (2019), https://doi.org/10.1158/1078-0432.ccr-19-2580

[29] R.S. Finn, J. Dering, D. Conklin, O. Kalous, D.J. Cohen, A.J. Desai, C. Ginther, M. Atefi, I. Chen, C. Fowst, G. Los, D.J. Slamon, PD 0332991, a selective cyclin D kinase 4/6 inhibitor, preferentially inhibits proliferation of luminal estrogen receptor-positive human breast cancer cell lines in vitro, Breast Cancer Res 11 (2009) 1–13, https://doi.org/10.1186/bcr2419

[30] J.A. Beaver, L. Amiri-Kordestani, R. Charlab, W. Chen, T. Palmby, A. Tilley, J.F. Zirkelbach, J. Yu, Q. Liu, L. Zhao, J. Crich, X.H. Chen, M. Hughes, E. Bloomquist, S. Tang, R. Sridhara, P.G. Kluetz, G. Kim, A. Ibrahim, R. Pazdur, P. Cortazar, FDA approval: palbociclib for the treatment of postmenopausal patients with es- trogen receptor-positive, HER2-negative metastatic breast cancer, Clin. Cancer Res 21 (2015) 4760–4766, https://doi.org/10.1158/1078-0432.CCR-15-1185

[31] A.J. Walker, S. Wedam, L. Amiri-Kordestani, E. Bloomquist, S. Tang, R. Sridhara, W. Chen, T.R. Palmby, J. Fourie Zirkelbach, W. Fu, Q. Liu, A. Tilley, G. Kim, P.G. Kluetz, A.E. McKee, R. Pazdur, FDA approval of palbociclib in combination with fulvestrant for the treatment of hormone receptor-positive, HER2-negative metastatic breast cancer, Clin. Cancer Res 22 (2016) 4968–4972, https://doi.org/ 10.1158/1078-0432.CCR-16-0493

[32] J. Chang, Y. Wang, L. Shao, R.M. Laberge, M. Demaria, J. Campisi, K. Janakiraman, N.E. Sharpless, S. Ding, W. Feng, Y. Luo, X. Wang, N. Aykin-Burns, K. Krager, U. Ponnappan, M. Hauer-Jensen, A. Meng, D. Zhou, Clearance of senescent cells by ABT263 rejuvenates aged hematopoietic stem cells in mice, Nat. Med. 22 (2016) 78–83, https://doi.org/10.1038/nm.4010

[33] T.J. Bussian, A. Aziz, C.F. Meyer, B.L. Swenson, J.M. van Deursen, D.J. Baker, Clearance of senescent glial cells prevents tau-dependent pathology and cog- nitive decline, Nature 562 (2018) 578–582, https://doi.org/10.1038/s41586-018- 0543-y

[34] H.-N.N. Kim, J. Chang, L. Shao, L. Han, S. Iyer, S.C. Manolagas, C.A. O'Brien, R.L. Jilka, D. Zhou, M. Almeida, DNA damage and senescence in osteoprogenitors expressing Osx1 may cause their decrease with age, Aging Cell 16 (2017) 693–703, https://doi.org/10.1111/acel.12597

[35] Y. Zhu, T. Tchkonia, H. Fuhrmann-Stroissnigg, H.M. Dai, Y.Y. Ling, M.B. Stout, T. Pirtskhalava, N. Giorgadze, K.O. Johnson, C.B. Giles, J.D. Wren, L.J. Niedernhofer, P.D. Robbins, J.L. Kirkland, Identification of a novel senolytic agent, navitoclax, targeting the Bcl-2 family of anti-apoptotic factors, Aging Cell 15 (2016) 428–435, https://doi.org/10.1111/acel.12445

[36] A. Agostini, L. Mondragón, A. Bernardos, R. Martínez-Máñez, M. Dolores Marcos, F. Sancenõn, J. Soto, A. Costero, C. Manguan-García, R. Perona, M. Moreno-Torres, R. Aparicio-Sanchis, J.R. Murguía, L. Mondragon, A. Bernardos, R. Martinez- Mañez, M. Dolores Marcos, F. Sancenon, J. Soto, A. Costero, C. Manguan-Garcia, R. Perona, M. Moreno-Torres, R. Aparicio-Sanchis, J.R. Murguia, Targeted cargo delivery in senescent cells using capped mesoporous silica nanoparticles, Angew. Chem. Int. Ed. 51 (2012) 10556–10560, https://doi.org/10.1002/anie.201204663

[37] D. Muñoz-Espín, M. Rovira, I. Galiana, C. Giménez, B. Lozano-Torres, M. Paez- Ribes, S. Llanos, S. Chaib, M. Muñoz-Martín, A.C. Ucero, G. Garaulet, F. Mulero, S.G. Dann, T. VanArsdale, D.J. Shields, A. Bernardos, J.R. Murguía, R. Martínez-Máñez, M. Serrano, A versatile drug delivery system targeting senescent cells, EMBO Mol. Med. 10 (2018) e9355, https://doi.org/10.15252/emmm.201809355

[38] I. Galiana, B. Lozano-Torres, M. Sancho, M. Alfonso, A. Bernardos, V. Bisbal, M. Serrano, R. Martínez-Máñez, M. Orzáez, Preclinical antitumor efficacy of se- nescence-inducing chemotherapy combined with a nanoSenolytic, J. Control. Release 323 (2020) 624–634, https://doi.org/10.1016/j.jconrel.2020.04.045

[39] B. Lozano-Torres, J.F. Blandez, I. Galiana, A. García-Fernández, M. Alfonso, M.D. Marcos, M. Orzáez, F. Sancenón, R. Martínez-Máñez, Real-time in vivo de- tection of cellular senescence through the controlled release of the NIR fluor- escent dye nile blue, Angew. Chem. Int. Ed. 59 (2020) 15152–15156, https://doi. org/10.1002/anie.202004142

[40] V. Apostolopoulos, G.A. Pietersz, I.F.C. McKenzie, MUC1 and breast cancer, Curr. Opin. Mol. Ther. 1 (1999) 98–103.

[41] G. Vivo-Llorca, V. Candela-Noguera, M. Alfonso, A. García-Fernández, M. Orzáez, F. Sancenón, R. Martínez-Máñez, M.U.C.1 Aptamer-Capped Mesoporous, Silica nanoparticles for navitoclax resistance overcoming in triple-negative, Breast Cancer, Chem. A Eur. J. 26 (2020) 16318–16327, https://doi.org/10.1002/chem.202001579

[42] J. Taylor-Papadimitriou, J. Burchell, D.W. Miles, M. Dalziel, MUC1 and cancer, Biochim. Biophys. Acta 1455 (1999) 301–313, https://doi.org/10.1016/s0925-4439(99)00055-1

[43] C. Giménez, C. De La Torre, M.M. Gorbe, E. Aznar, F. Sancenón, J.R. Murguía, R. Martínez-Máñez, M.D. Marcos, P. Amorós, C. Gim??nez, C. De La Torre, M.M. Gorbe, E. Aznar, F. Sancen??n, J.R. Murgu??a, R. Mart??nez-M????ez, M.D. Marcos, P. Amor??s, Gated mesoporous silica nanoparticles for the con- trolled delivery of drugs in cancer cells, Langmuir 31 (2015) 3753–3762, https:// doi.org/10.1021/acs.langmuir.5b00139

[44] A. Bernardos, L. Mondragón, E. Aznar, M.D. Marcos, R. Martínez-Máñez, F. Sancenón, J. Soto, J.M. Barat, E. Pérez-Payá, C. Guillem, P. Amorós, Enzyme- responsive intracellular controlled release using nanometric silica mesoporous supports capped with "saccharides, ACS Nano 4 (2010) 6353–6368, https://doi. org/10.1021/nn101499d

[45] D.P. Jones, J.L. Carlson, P.S. Samiec, P. Sternberg, V.C. Mody, R.L. Reed, L.A.S. Brown, Glutathione measurement in human plasma. Evaluation of sample collection, storage and derivatization conditions for analysis of dansyl deriva- tives by HPLC, Clin. Chim. Acta 275 (1998) 175–184, https://doi.org/10.1016/ S0009-8981(98)00089-8

[46] L. Pascual, C. Cerqueira-Coutinho, A. García-Fernández, B. de Luis, E.S. Bernardes, M.S. Albernaz, S. Missailidis, R. Martínez-Máñez, R. Santos-Oliveira, M. Orzaez, F. Sancenón, MUC1 aptamer-capped mesoporous silica nanoparticles for con- trolled drug delivery and radio-imaging applications, Nanomed. Nanotechnol., Biol. Med 13 (2017) 2495–2505, https://doi.org/10.1016/j.nano.2017.08.006

[47] S.J. Gendler, MUC1, The renaissance molecule, J. Mammary Gland Biol. Neoplasia 2001 (63) (2001) 339–353, https://doi.org/10.1023/A:1011379725811

[48] B. Lozano-Torres, A. Estepa-Fernández, M. Rovira, M. Orzáez, M. Serrano, R. Martínez-Máñez, F. Sancenón, The chemistry of senescence, Nat. Rev. Chem. 3 (2019) 426–441, https://doi.org/10.1038/s41570-019-0108-0

[49] S. Goel, M.J. DeCristo, S.S. McAllister, J.J. Zhao, CDK4/6 inhibition in cancer: be- yond cell cycle arrest, Trends Cell Biol. 28 (2018) 911–925, https://doi.org/10. 1016/j.tcb.2018.07.002

[50] N. Zamzami, P. Marchetti, M. Castedo, C. Zanin, J.L. Vayssière, P.X. Petit, G. Kroemer, Reduction in mitochondrial potential constitutes an early irrever- sible step of programmed lymphocyte death in vivo, J. Exp. Med 181 (1995) 1661, https://doi.org/10.1084/JEM.181.5.1661

[51] R. Overbeeke, M. Yildirim, C.P.M. Reutelingsperger, C. Haanen, I. Vermes, Sequential occurrence of mitochondrial and plasma membrane alterations, fluctuations in cellular Ca2+ and pH during initial and later phases of cell death, Apoptosis 4 (1999) 455–460, https://doi.org/10.1023/A:1009604510329

[52] J.H. Park, L. Gu, G. Von Maltzahn, E. Ruoslahti, S.N. Bhatia, M.J. Sailor, Biodegradable luminescent porous silicon nanoparticles for in vivo applications, 2009, Nat. Mater. 84 (8) (2009) 331–336, https://doi.org/10.1038/nmat2398

[53] M. Yu, J. Zheng, Clearance pathways and tumor targeting of imaging nano- particles, ACS Nano 9 (2015) 6655–6674, https://doi.org/10.1021/acsnano. 5b01320

[54] Y.-N. Zhang, W. Poon, A.J. Tavares, I.D. McGilvray, W.C.W. Chan, Nanoparticle–liver interactions: cellular uptake and hepatobiliary elimination, J. Control. Release 240 (2016) 332–348, https://doi.org/10.1016/j.jconrel.2016.01.020

[55] E. González-Gualda, M. Pàez-Ribes, B. Lozano-Torres, D. Macias, J.R. Wilson, C. González-López, H.L. Ou, S. Mirón-Barroso, Z. Zhang, A. Lérida-Viso, J.F. Blandez, A. Bernardos, F. Sancenón, M. Rovira, L. Fruk, C.P. Martins, M. Serrano, G.J. Doherty, R. Martínez-Máñez, D. Muñoz-Espín, Galacto-con- jugation of Navitoclax as an efficient strategy to increase senolytic specificity and reduce platelet toxicity, Aging Cell 19 (2020) 1–19, https://doi.org/10.1111/ acel.13142

[56] I. Melero, E. Castanon, M. Alvarez, S. Champiat, A. Marabelle, Intratumoural ad- ministration and tumour tissue targeting of cancer immunotherapies, Nat. Rev. Clin. Oncol. 18 (2021) 558–576, https://doi.org/10.1038/S41571-021-00507-Y

[57] A. Al Shoyaib, S.R. Archie, V.T. Karamyan, Intraperitoneal route of drug admin- istration: should it be used in experimental animal studies, Pharm. Res. 37 (2019) 12, https://doi.org/10.1007/S11095-019-2745-X

[58] K. Chaudhary, S. Haddadin, R. Nistala, C. Papageorgio, Intraperitoneal drug therapy: an advantage, Curr. Clin. Pharmacol. 5 (2010) 82–88, https://doi.org/10. 2174/157488410791110779

[59] D. O'Reilly, M. Al Sendi, C.M. Kelly, Overview of recent advances in metastatic triple negative breast cancer, World J. Clin. Oncol. 12 (2021) 164–182, https://doi. org/10.5306/wjco.v12.i3.164

[60] D. Muñoz-Espín, M. Serrano, Cellular senescence: from physiology to pathology, Nat. Rev. Mol. Cell Biol. 15 (2014) 482–496, https://doi.org/10.1038/nrm3823

[61] R.R.S. Finn, J.P.J. Crown, I. Lang, K. Boer, I.M. Bondarenko, S.O. Kulyk, J. Ettl, R. Patel, T. Pinter, M. Schmidt, Y. Shparyk, A.R. Thummala, N.L. Voytko, C. Fowst, X. Huang, S.T. Kim, S. Randolph, D.J. Slamon, et al., The cyclin-dependent kinase 4/6 inhibitor palbociclib in combination with letrozole versus letrozole alone as first-line treatment of oestrogen receptor-positive, HER2-negative, advanced breast cancer (PALOMA-1/TRIO-18): a randomised phase 2 study, Lancet Oncol. 16 (2015) 25–35, https://doi.org/10.1016/S1470-2045(14)71159-3

[62] R.S. Finn, M. Martin, H.S. Rugo, S. Jones, S.-A. Im, K. Gelmon, N. Harbeck, O.N. Lipatov, J.M. Walshe, S. Moulder, E. Gauthier, D.R. Lu, S. Randolph, V. Diéras, D.J. Slamon, Palbociclib and letrozole in advanced breast cancer, New Engl. J. Med.

375 (2016) 1925–1936, https://doi.org/10.1056/NEJMoa1607303
[63] D.W. Fry, P.J. Harvey, P.R. Keller, W.L. Elliott, M. Meade, E. Trachet, M. Albassam, X. Zheng, W.R. Leopold, N.K. Pryer, P.L. Toogood, Specific inhibition of cyclin- dependent kinase 4/6 by PD 0332991 and associated antitumor activity in human tumor xenografts, Mol. Cancer Ther. 3 (2004) 1427–1438.
[64] S. Pernas, S.M. Tolaney, E.P. Winer, S. Goel, CDK4/6 inhibition in breast cancer: current practice and future directions, Ther. Adv. Med. Oncol. 10 (2018), https:// doi.org/10.1177/1758835918786451
[65] N. Ohtani, A. Takahashi, D.J. Mann, E. Hara, Cellular senescence: a double-edged sword in the fight against cancer, Exp. Dermatol. 21 (2012) 1–4, https://doi.org/ 10.1111/j.1600-0625.2012.01493.x
[66] S.G. Rao, J.G. Jackson, SASP: tumor suppressor or promoter? Yes, Trends Cancer 2 (2016) 676–687, https://doi.org/10.1016/j.trecan.2016.10.001
[67] Y. Zhu, T. Tchkonia, T. Pirtskhalava, A.C. Gower, H. Ding, N. Giorgadze, A.K. Palmer, Y. Ikeno, G.B. Hubbard, M. Lenburg, S.P. O'Hara, N.F. LaRusso, J.D. Miller, C.M. Roos, G.C. Verzosa, N.K. LeBrasseur, J.D. Wren, J.N. Farr, S. Khosla, M.B. Stout, S.J. McGowan, H. Fuhrmann-Stroissnigg, A.U. Gurkar, J. Zhao, D. Colangelo, A. Dorronsoro, Y.Y. Ling, A.S. Barghouthy, D.C. Navarro, T. Sano, P.D. Robbins, L.J. Niedernhofer, J.L. Kirkland, The Achilles' heel of senescent cells: from transcriptome to senolytic drugs, Aging Cell. 14 (2015) 644–658, https:// doi.org/10.1111/acel.12344
[68] A. Soto-Gamez, M. Demaria, Therapeutic interventions for aging: the case of cellular senescence, Drug Discov. Today 22 (2017) 786–795, https://doi.org/10. 1016/j.drudis.2017.01.004